Quantum and Classical Correlations in Open Quantum Spin Lattices via Truncated-Cumulant Trajectories

Wouter Verstraelen,[1,2,*,†] Dolf Huybrechts,[2,3,†] Tommaso Roscilde,[3] and Michiel Wouters[2]

[1] *Division of Physics and Applied Physics, School of Physical and Mathematical Sciences, Nanyang Technological University, Singapore 637371, Singapore*

[2] *TQC, Universiteit Antwerpen, Universiteitsplein 1 Antwerpen B-2610, Belgium*

[3] *Univ Lyon, Ens de Lyon, CNRS, Laboratoire de Physique, Lyon F-69342, France*

(Received 11 October 2022; accepted 15 June 2023; published 12 July 2023)

The study of quantum many-body physics in Liouvillian open quantum systems becomes increasingly important with the recent progress in experimental control on dissipative systems and their exploitation for technological purposes. A central question in open quantum systems concerns the fate of quantum correlations, and the possibility of controlling them by engineering the competition between the Hamiltonian dynamics and the coupling of the system to a bath. Such a question is very challenging from a theoretical point of view, as numerical methods faithfully accounting for quantum correlations are either relying on exact diagonalization, drastically limiting the sizes that can be treated numerically, or on approximations on the range or strength of quantum correlations, associated with the choice of a specific ansatz for the density matrix. In this work we propose a new method to treat open quantum spin lattices, based on stochastic quantum trajectories for the solution of the open-system dynamics. Along each trajectory, the hierarchy of equations of motion for many-point spin-spin correlators is truncated to a given finite order, assuming that multivariate kth-order cumulants vanish for k exceeding a cutoff k_c. This scheme allows one to track the evolution of quantum spin-spin correlations up to order k_c for all length scales. We validate this approach in the paradigmatic case of the dissipative phase transitions of the two-dimensional XYZ lattice subject to spontaneous decay. We convincingly assess the existence of steady-state phase transitions from paramagnetic to ferromagnetic, and back to paramagnetic, upon increasing one of the Hamiltonian spin-spin couplings, as well as the classical Ising nature of such transitions. Moreover, the approach allows us to show the presence of significant quantum correlations in the vicinity of the dissipative critical point, and to unveil the presence of spin squeezing, which can be proven to be a tight lower bound to the quantum Fisher information.

DOI: 10.1103/PRXQuantum.4.030304

I. INTRODUCTION

After many decades of remarkable successes in describing nature at the microscopic level, and in providing foundational contributions to modern technology, the frontier of research on quantum mechanics has turned in the last decade to the hitherto impossible creation and manipulation of quantum entanglement at large scales, constituting the basis of the so-called second quantum revolution [1,2]. The main technological rewards of this revolution are expected to lie in sensing, communication, and information processing [3,4]. A most important challenge in this endeavor stems from the interaction of quantum systems with their environment, which generally destroys quantum superpositions, namely, the fundamental resource for quantum technology tasks. This calls for a detailed understanding of the interaction of complex quantum systems with their environment, and for the devising of strategies to overcome decoherence. The most obvious remedy is to limit the interaction with the environment as much as possible, but an alternative strategy is to investigate the possibility of creating interesting quantum states by engineering the environment itself [5,6].

A promising setting for the nonunitary manipulation of quantum states is that of a phase transition in a driven-dissipative many-body system [7–17]. On the experimental side, several platforms have been developed where the physics of nonequilibrium quantum steady states can be

*wouter.verstraelen@ntu.edu.sg

†These authors contributed equally.

studied. One could cite circuit QED [18], arrays of Rydberg atoms [19], ion traps [20], and semiconductor microcavities [21], to name only the most advanced setups. In analogy with equilibrium statistical physics, theoretical understanding often benefits from using "toy models" able to capture fundamental phenomena. For driven-dissipative systems, the main models under study are Bose-Hubbard-type models that are used to describe photonic systems undergoing photon loss [22], and spin models that can, for instance, provide an effective description of Rydberg atoms undergoing spontaneous decay [23]. As possible applications of correlations in driven-dissipative lattice-like geometries beyond simulation, we can mention efficient solving of NP-hard optimization problems [24], related to neural networks [25–27] and metrology [28], among others. Even in the case of the simplest models, our theoretical understanding of phase transitions in driven-dissipative systems is hampered both by the absence of a free energy minimization principle, underpinning the determination of the steady state, and by the difficulty to simulate systems that are sufficiently large to approach the thermodynamic limit. In order to address these challenges, a new set of theoretical tools have been developed over the last years [8,29–37] for the study of open quantum many-body systems. It is to the development of new methods that the present paper wishes to contribute. Here we propose a scheme for dissipative quantum spin lattices that effectively combines the stochastic sampling of the density matrix evolution by the quantum trajectory method with a scheme of truncation of the correlation-function hierarchy to second order. Our method is inspired by approaches already developed in the case of bosonic lattice models [9,35,36], in which stochastic quantum trajectories are combined with a Gaussian ansatz on the single-trajectory bosonic state—the latter state can be viewed as resulting from the ansatz of vanishing cumulants of the bosonic fields beyond second-order ones. Similarly, we adopt here for the spin operators a truncation of the correlation hierarchy, by assuming that cumulants of order k exceeding a given cutoff k_c vanish—in practice, we take $k_c = 2$ in this work, but the same approach can be readily extended to higher-order truncation schemes. The rationale behind the truncation is that higher-order correlations, while developing in closed quantum systems, are far more vulnerable to decoherence in open ones, so that their influence on the dynamics remains limited [38]. Our method is sufficiently simple to treat quite large systems comprising hundreds of qubits, and at the same time it allows in principle for a faithful description of long-range quantum correlations, which is a fundamental requirement in order to describe phase transitions that are either driven or significantly altered by quantum effects.

As an illustration of our approach, we apply our method to the driven-dissipative *XYZ* model in two spatial dimensions, which can effectively describe the dynamics of an array of optically driven Rydberg atoms [23], and which has attracted considerable attention on the theory level as an effective model for driven-dissipative phase transitions [39–53]. It combines anisotropic nearest-neighbor couplings with spin-flip dissipation, and, in spite of its simplicity, it gives rise to a very rich phase diagram, already at the mean-field level [23]. Moreover, it has become clear that the mean-field predictions are qualitatively wrong in some parameter regimes [39,41,44], pointing at the fundamental role of correlations, and posing the challenge to their faithful description. Here we find that the simplest nontrivial formulation of our method, focusing on two-point quantum correlators, leads to surprisingly good agreement with the exact predictions for small systems, and shows a clear trend of improvement with increasing system size. Using finite-size scaling, we are able to characterize the phase transitions present in the dissipative *XYZ* system, and confirm that they belong to the two-dimensional (2D) classical Ising universality class. This result is to be contrasted with that obtained by simply including classical correlations within a mean-field trajectory scheme (corresponding to $k_c = 1$ in the cumulant-truncation approach introduced below), whose results for the transition are inconsistent with the 2D Ising universality class. This observation suggests a surprisingly crucial role of quantum correlations (fully discarded in the $k_c = 1$ scheme, and accounted for at all length scales in the $k_c = 2$ one) in determining the critical behavior of the open quantum system, in spite of the apparent classical nature of the observed criticality. Furthermore, we inspect the nature of quantum correlations and observe that the system develops spin squeezing in the steady state, witnessing short-range entanglement. Moreover, we analyze an upper bound of the quantum Fisher information based on a convex-roof construction [54], and show that spin squeezing comes close to saturating this bound in the vicinity of the dissipative phase transition.

Our paper is structured as follows. In Sec. II, we describe the dissipative *XYZ* model under study, and review previous numerical approaches used to study this and other dissipative many-body models. In Sec. III, we present the details of the correlation-hierarchy method for dissipative spin systems. Section IV is devoted to the discussion of the results, and in particular of the finite-size scaling analysis of the dissipative phase transition, as well as of the quantum correlation properties across the phase diagram. Conclusions are offered in Sec. V.

II. DISSIPATIVE QUANTUM SPIN LATTICES

A. The dissipative *XYZ* model

We focus our attention on the two-dimensional dissipative *XYZ* Heisenberg model, which has been the subject of intensive theoretical research efforts in the past years [23,39–53], due to its rich phase diagram. Its coherent dynamics is governed by the anisotropic Heisenberg

Hamiltonian

$$\hat{H} = \sum_{\langle i,j \rangle} (J_x \hat{\sigma}_i^x \hat{\sigma}_j^x + J_y \hat{\sigma}_i^y \hat{\sigma}_j^y + J_z \hat{\sigma}_i^z \hat{\sigma}_j^z). \tag{1}$$

Here the J_α are the coupling strengths for the $\alpha = x, y, z$ spin components of nearest-neighboring spins, the $\hat{\sigma}_i^\alpha$ are the Pauli matrices acting on site i, and $\sum_{\langle ij \rangle}$ runs over all pairs of nearest neighbors $\langle ij \rangle$. The XYZ couplings can be engineered in, e.g., Rydberg or dipolar atoms, through a combination of dipole interactions with engineered optical pumping [23]. Note that energy minimization alone would favor antiferromagnetic order for positive values of the coupling constants, and ferromagnetic order when they are all negative; yet the steady state of the dissipative dynamics challenges the prediction of energy minimization, and it exposes its fundamental nonequilibrium nature.

The dissipative part of the dynamics stems from spontaneous decay, described as incoherent spin flips along the z axis. Each spin is coupled to its own Markovian environment, so that the equation governing the dissipative dynamics of the quantum state $\hat{\rho}$ can be assumed to be of Gorini-Kossakowski-Sudarshan-Lindblad (GKSL) form [55–57]

$$\partial_t \hat{\rho} = -i[\hat{H}, \hat{\rho}] + \frac{1}{2} \sum_j (2\hat{\Gamma}_j \hat{\rho} \hat{\Gamma}_j^\dagger - \hat{\Gamma}_j^\dagger \hat{\Gamma}_j \hat{\rho} - \hat{\rho} \hat{\Gamma}_j^\dagger \hat{\Gamma}_j). \tag{2}$$

Here, the $\hat{\Gamma}_j = \sqrt{\gamma} \hat{\sigma}_j^- = \sqrt{\gamma}(\hat{\sigma}_j^x - i\hat{\sigma}_j^y)/2$ are the Lindblad operators for the incoherent spin-flip processes along the z axis with dissipation rate γ. The description of spontaneous decay in quantum optics by the GKSL equation is widely accepted [57], and initiated in Ref. [23] for the study of the dissipative XYZ model. We note that in more general open quantum systems, this validity is not always true [58], but it can often be justified through collisional models [59,60], especially in cases where external driving is present.

Along the dynamics governed by master equation (2), the expectation value of an operator evolves according to the equation

$$d\langle \hat{O} \rangle = i\langle [\hat{H}\hat{O}] \rangle dt - \frac{1}{2} \sum_j (\langle \hat{\Gamma}_j^\dagger [\hat{\Gamma}_j \hat{O}] \rangle - \langle [\hat{\Gamma}_j^\dagger \hat{O}] \hat{\Gamma}_j \rangle) dt, \tag{3}$$

from which the time evolution of the moments of the spin operators can be straightforwardly constructed.

A pioneering mean-field study of the XYZ model [23], based on the assumption of a fully factorized quantum state $\hat{\rho} = \bigotimes_i \hat{\rho}_i$ at all times, has revealed a very rich phase diagram, containing a paramagnetic phase, a ferromagnetic phase, an antiferromagnetic phase, as well as a spin-density wave and a staggered XY phase. Subsequent works, based on methods going beyond a single-site mean-field approach, offer substantially different predictions for the phase diagram when the XYZ model is cast on a two-dimensional lattice. Cluster mean-field descriptions on the level of the master equation [39,43,47,61], which are able to incorporate the influence of some short-range quantum and classical correlations, revealed a drastic impact of such correlations on the phase diagram of the system, a feature not observed in their closed-system counterparts. However, as such, they completely miss the long-range fluctuations, which actually govern the critical behavior.

On the other hand, the mean-field approximation applied at the level of the quantum trajectory formalism—namely, by studying each trajectory via a Gutzwiller ansatz—allows for the inclusion of long-range *classical* correlations [41], possibly combined with some short-range quantum correlations when using a cluster Gutzwiller wave function [44]. Unfortunately, in all cluster approaches—both at the level of the master equation as well as at the level of quantum trajectories—one is still limited by the relatively small size of the clusters that can be used, and the faithful description of correlations is therefore not guaranteed. Moreover, as we shall see in this work, the critical behavior predicted by Gutzwiller trajectories is very different from what one can obtain with improved methods, taking into account quantum correlations to all scales.

It is worth mentioning that the dissipative XYZ model is efficiently solvable in the case of all-to-all connectivity, corresponding to a system in infinite spatial dimensions [46]. The efficient solution, allowing one to exactly treat systems with hundreds of spins, exploits the permutational symmetry of the system in infinite dimensions and it has been used to test the validity of the mean-field approximation in this limit [46]. Some extensions to frustrated lattice geometries were studied in Refs. [47,52] on the mean-field or cluster mean-field level. The literature has so far predominantly focused on the transition from the paramagnetic phase to the ferromagnetic phase, which, e.g., takes place for $J_y \approx \gamma$ when one chooses $J_x = 0.9\gamma$ and $J_z = \gamma$.

Using beyond-mean-field methods (see the following section), Refs. [40,43,61] provided estimates of the critical exponent $\gamma \approx 1.5$, which clearly indicates a departure from mean-field prediction. However, the convergence of these results is hard to assess and could therefore either be interpreted as hinting towards a known set of exponents such as those of the Ising universality class [40], or pointing to a new class on its own [61]. Extensions to the initial mean-field study in Ref. [23], as well as exact numerical methods in small systems [42], have suggested a reentrant behavior: upon increasing the value of J_y further, ferromagnetic order is lost, and the system reenters into a paramagnetic phase. The study of this second transition and of its critical properties, however, is not a simple task.

Interestingly, some of the methods either did not observe the reentrant behavior or suggested that it was not associated with a true phase transition [40,42,45]. Most of the beyond-mean-field methods are limited by system size, or do not converge in this region of high J_y, where it has been shown that the state is highly mixed [39,40,46].

In the following sections we see that our method allows us to overcome the above difficulties, and to provide a quantitative analysis of all the transitions of the system on large lattices (comprising up to hundreds of spins), as well as an assessment of the importance of quantum correlations.

B. Numerical techniques for the study of dissipative spin lattices

Before ending this section we survey other numerical approaches that have been developed for the study of dissipative quantum spin models in the recent past (see also Ref. [30] for a recent review), and which have been or could be applied to the study of dissipative phase transitions such as those of the *XYZ* model.

Several methods have been proposed in order to overcome the limitations of cluster mean-field approaches, based on different ansatzes for the density matrix solving the Lindblad master equation. One such method is the corner-space renormalization method [32,40], which searches for a solution of the master equation for a given system size within a reduced Hilbert subspace, built from the most likely pure states appearing in the steady state of a smaller system size. Such a method allows one to *a priori* account for quantum correlations encompassing the whole system; yet, due to the choice of a reduced Hilbert space growing polynomially with system size, it is limited in the amount of entropy that the steady state can exhibit. Recently, variational ansatzes based on neural network quantum states [45,62–64] have also been proposed, showing promise for the description of large lattices; application to the dissipative *XYZ* model has not shown the reentrant paramagnetic behavior [45]. Another class of ansatzes is offered by tensor network states [29,30]: within this approach, infinite projected entangled pair states are particularly relevant, as they immediately grant access to the thermodynamic limit in the regions where they converge [48,49]. Application to the dissipative *XYZ* model has been considered in Ref. [65]. It has been found however that this approach is subject to instabilities [48]. Attempts to overcome this issue have been suggested [48,49], but have not to our knowledge been tested in the general dissipative *XYZ* model. Generally speaking, tensor network states have shown to be most effective for the study of 1D systems [29].

Finally, an alternative category of methods for dissipative spin lattices relies on the truncated Wigner approximation (TWA) [37,66,67], which represents the expectation values of operators along the quantum dynamics as averages over evolutions of classical spins, starting from states drawn out of the discrete Wigner distribution for the quantum spins. This approach can tackle very large lattice sizes and effectively account for classical correlations, but it has the disadvantage that the quantum nature of the system is mimicked by classical fluctuations and it is therefore unclear whether quantum effects are properly described in the steady state. For example, the TWA has been shown to suffer from unphysical predictions for the single-photon-driven Bose-Hubbard model [68] and also to miss the phase transition in the steady state under two-photon driving [35], motivating the construction of techniques that are complementary to the TWA.

III. CORRELATION HIERARCHIES FOR DISSIPATIVE SYSTEMS

A. Open quantum systems: quantum trajectories, classical versus quantum fluctuations

1. Stochastic unraveling of the open-system evolution

The most fundamental level of description for the dynamics of quantum systems coupled to a Markovian bath is offered by GKSL equation (2) [57,69–72] for the evolution of the density matrix of the system. Nonetheless, the theoretical framework which we use here is that of quantum trajectories [29], which stochastically sample the density matrix. In order to understand this framework, one should realize that master equation (2) is largely independent of the environment specifics. We may thus replace the true environment with a macroscopic measuring device without an observer. In practical terms, this means that the incoherent effect of the environment is the same as the one that would arise from a continuous weak, nonselective measurement. It is precisely because the measurement is not read out that classical uncertainty over the system increases and Eq. (2) does not conserve purity. But one may also consider what happens if one does observe the state of the measuring device. The time evolution is then conditioned on the measurement result, and, assuming no measurement imperfections, there is no loss of information, so that states remain pure. Such a conditional evolution consists of *quantum trajectories*, which were introduced in the seminal works of Refs. [73–76]. The expectation values associated with the density matrix evolved with master equation (2) are then recovered by averaging over the pure states of the trajectories (that is, tracing out the information on the measurement outcome), in the limit of a sufficiently large sample. This latter approach is known in the literature as the wave-function Monte Carlo method, or the stochastic sampling method. The advantage of the wave-function Monte Carlo method, compared to the direct solution of the master equation, is that the pure states of the trajectories can be described by

a wave function $|\psi\rangle \in \mathcal{H}$ with $D = \dim(\mathcal{H})$ components only, compared to a density matrix $\hat{\rho} \in \mathcal{H} \otimes \mathcal{H}^*$ with D^2 components, so that significantly less computer memory is required for the exact numerical simulation of trajectories.

Within this picture of quantum trajectories, there is still some freedom regarding the (possibly hypothetical) measurement protocol that is performed, defining a so-called *unraveling* scheme. As long as no additional approximations are made, the result of averaging over trajectories should be consistent with the master equation independently of the measurement protocol, even though the individual trajectories may have a vastly different behavior depending on the measurement protocol itself.

One of the most adopted unraveling schemes is based on quantum jumps (which models, e.g., photon counting in experiments on optical cavities), leading to trajectories of the form

$$d|\widetilde{\psi}\rangle = -i\hat{\mathrm{H}}_{\mathrm{traj}}|\widetilde{\psi}\rangle dt, \tag{4}$$

where

$$\hat{\mathrm{H}}_{\mathrm{traj}} = \hat{\mathrm{H}} - \frac{i}{2}\sum_j \hat{\Gamma}_j^\dagger \hat{\Gamma}_j \tag{5}$$

is an effective non-Hermitian Hamiltonian. Equation (4) does not conserve the norm of the wave function; indicated by the tilde notation. This evolution is complemented by the fact that, given a uniform stochastic random number $0 < \zeta < 1$, whenever $\||\widetilde{\psi}\rangle\|^2 < \zeta$, a discrete jump of the form

$$|\widetilde{\psi}\rangle \xrightarrow{\text{jump}} \frac{\hat{\Gamma}_l|\widetilde{\psi}\rangle}{\|\hat{\Gamma}_j|\widetilde{\psi}\rangle\|} \tag{6}$$

will take place, where the choice of $\hat{\Gamma}_l$ has probability $\|\hat{\Gamma}_l|\widetilde{\psi}\rangle\|^2/\sum_j \|\hat{\Gamma}_j|\widetilde{\psi}\rangle\|^2$. In the case of quantum spin models with spontaneous decay, such a scheme corresponds to having a photon counting apparatus coupled to each spin separately, measuring the number of photons spontaneously emitted by the spin.

A different type of unraveling is obtained by a different measurement scheme, which in quantum optics corresponds to heterodyning—namely, mixing the emitted photons with a classical field at a different frequency. For heterodyne detection, the single-trajectory evolution is governed by a stochastic Schrödinger equation of the form

$$\begin{aligned} d|\psi\rangle = &-i\hat{H}dt\,|\psi\rangle \\ &+ \sum_j \left(\langle\hat{\Gamma}_j^\dagger\rangle\hat{\Gamma}_j - \frac{1}{2}\langle\hat{\Gamma}_j^\dagger\rangle\langle\hat{\Gamma}_j\rangle - \frac{1}{2}\hat{\Gamma}_j^\dagger\hat{\Gamma}_j\right)dt\,|\psi\rangle \\ &+ \sum_j (\hat{\Gamma}_j - \langle\hat{\Gamma}_j\rangle)dZ_j^*\,|\psi\rangle\,, \end{aligned} \tag{7}$$

where $dZ_j = (dW_j^X + i dW_j^Y)/\sqrt{2}$ is complex Wiener noise in the Ito sense, satisfying $dZ_i^* dZ_j = \delta_{ij}\,dt, dZ_i dZ_j = 0$. Such an evolution is often referred to as quantum state diffusion [77]. For the evolution of expectation values, Eq. (7) yields

$$\begin{aligned} d\langle\hat{\mathrm{O}}\rangle = &\, i\langle[\hat{\mathrm{H}}\hat{\mathrm{O}}]\rangle dt \\ &- \frac{1}{2}\sum_j (\langle\hat{\Gamma}_j^\dagger[\hat{\Gamma}_j\hat{\mathrm{O}}]\rangle - \langle[\hat{\Gamma}_j^\dagger\hat{\mathrm{O}}]\hat{\Gamma}_j\rangle)dt \\ &+ \sum_j (\langle\hat{\Gamma}_j^\dagger(\hat{O} - \langle\hat{O}\rangle)\rangle dZ_j + \langle(\hat{O} - \langle\hat{O}\rangle)\hat{\Gamma}_j\rangle dZ_j^*). \end{aligned} \tag{8}$$

Comparing this expression with Eq. (3), we see that the time evolution for expectation values under the master equation is identical to the deterministic part of the evolution under the heterodyne quantum trajectories. The stochastic nature of the detector clicks under quantum trajectory evolution reflects itself in the addition of noise to the time evolution of expectation values.

2. Classical versus quantum fluctuations and correlations

Given the correspondence between the master equation and its stochastic unraveling, one has the choice to choose an ansatz at either level. We have already pointed out above the advantage of quantum trajectories in reducing the computational cost for exact calculations. The advantage of quantum trajectories is even more dramatic when an ansatz is made on the state of the system. Indeed, unlike the case of an ansatz for the density matrix, an ansatz formulated at the trajectory level is always complemented by classical (i.e., trajectory-to-trajectory) fluctuations [29]. Denoting by $|\psi_n(t)\rangle$ the solution of the stochastic Schrödinger equation along the nth trajectory, we define as classical fluctuations of an observable $\hat{O}$ its trajectory-to-trajectory fluctuations

$$\mathcal{F}_c(\hat{O}) = [O_n^2(t)]_{\mathrm{traj}} - [O_n(t)]_{\mathrm{traj}}^2, \tag{9}$$

where $O_n(t) = \langle\psi_n(t)|\hat{O}|\psi_n(t)\rangle$ is the single-trajectory expectation value of the observable, $[\cdot]_{\mathrm{traj}} = N_{\mathrm{traj}}^{-1}\sum_n(\cdot)$ denotes the average over N_{traj} trajectories, and the time t is chosen to be in the regime of convergence to the steady state. The above fluctuations are uniquely due to the effect of the environment, and they correspond to the incoherent part of the fluctuations associated with the pure-state decomposition of the density matrix

$$\rho(t) = \frac{1}{N_{\mathrm{traj}}}\sum_n |\psi_n(t)\rangle\langle\psi_n(t)|, \tag{10}$$

valid asymptotically in the limit $N_{\text{traj}} \to \infty$. On the other hand, quantum fluctuations in this context can be defined as the fluctuations proper to the single-trajectory wave functions $|\psi_n(t)\rangle$, averaged over all trajectories:

$$\mathcal{F}_q(\hat{O}) = [\langle O^2\rangle_n(t) - \langle O(t)\rangle_n^2]_{\text{traj}} \tag{11}$$

with $\langle O^2\rangle_n(t) = \langle\psi_n(t)|\hat{O}^2|\psi_n(t)\rangle$. These fluctuations are clearly most sensitive to the choice of the ansatz for the trajectory wave functions. It is easy to verify that the total fluctuations associated with the density matrix can be decomposed into a classical and a quantum part:

$$\mathcal{F}(\hat{O}) = \langle\hat{O}^2\rangle_{\hat{\rho}} - \langle\hat{O}\rangle_{\hat{\rho}}^2 = \mathcal{F}_c(\hat{O}) + \mathcal{F}_q(\hat{O}) \tag{12}$$

with $\langle\cdot\rangle_{\hat{\rho}} = \text{Tr}(\hat{\rho}\,\cdot)$. Note that the decomposition of the density matrix into pure states (and thus relative contributions of $\mathcal{F}_c$ and $\mathcal{F}_q$) is not unique, as it depends in principle on the stochastic unraveling that one chooses.

A similar decomposition can be carried out in the case of correlations, namely, given two local operators $\hat{A}$ and $\hat{B}$ (for instance, $\hat{A} = \hat{\sigma}_i^{\mu}$ and $\hat{B} = \hat{\sigma}_j^{\nu}$ for two local spin components),

$$C(\hat{A},\hat{B}) = \langle\hat{A}\hat{B}\rangle_{\hat{\rho}} - \langle\hat{A}\rangle_{\hat{\rho}}\langle\hat{B}\rangle_{\hat{\rho}} = C_c(\hat{A},\hat{B}) + C_q(\hat{A},\hat{B}), \tag{13}$$

where

$$C_c(\hat{A},\hat{B}) = [A_n(t)B_n(t)]_{\text{traj}} - [A_n(t)]_{\text{traj}}[B_n(t)]_{\text{traj}} \tag{14}$$

are the classical correlations associated with trajectory-to-trajectory fluctuations, while

$$C_q(\hat{A},\hat{B}) = [\langle AB\rangle_n(t) - A_n(t)B_n(t)]_{\text{traj}} \tag{15}$$

are referred to as the quantum correlations, originating from the entangled nature of the wave function of each trajectory.

The above discussion suggests that the stochastic unraveling is able to capture the essential traits of the classical, incoherent fluctuations and correlations of the density matrix solution to the master equation, regardless of the choice of ansatz wave function describing each trajectory (but the results of this work cast some doubts on this point of view; see Sec. IV D). This aspect has been revealed by several quantum trajectory calculations based on the Gutzwiller ansatz [41,78–81], the cluster Gutzwiller ansatz [33,44], the Gaussian ansatz [9,36], and the matrix-product state ansatz [82,83], generally providing superior results with respect to calculations based on similar ansatzes formulated at the level of the density matrix. As an example, a Gaussian ansatz for the trajectory wave functions of a bosonic system is able to describe phenomena such as optical bistability in dissipative nonlinear cavities that cannot be described by applying the same Gaussian ansatz at the level of the master equation [35,36]. Indeed, the Gaussian ansatz at the level of the master equation approximates the density matrix to be a single Gaussian state, fully described in terms of the average field quadratures and of their covariance matrix, while the Gaussian ansatz for trajectory wave functions approximates the density matrix as a pure-state decomposition on Gaussian states, which is no longer a Gaussian state—namely its higher-order correlations for the field quadratures are no longer reducible to one- and two-point ones.

In this work we apply similar insight to the case of quantum spin systems. The analog of a Gaussian state for a spin system is a state whose higher-order spin-spin correlations are reducible to single-spin and two-spin expectation values, assuming the vanishing of all multivariate cumulants for quantum spin operators beyond the second-order ones. We apply such an ansatz to single trajectories for the study of the evolution of dissipative quantum spin lattices in the next section. Before doing so, nonetheless, we elaborate further on the link between quantum fluctuations and correlations extracted from specific unraveling schemes, and quantum fluctuations and correlations associated with the full state $\hat{\rho}$ that is stochastically reconstructed by the unraveling scheme. This link is discussed in the next subsection.

3. Quantum correlations from trajectories versus the quantum Fisher information of the full state

The previous subsection showed that the quantum trajectory approach can shed light on the role of classical versus quantum fluctuations and correlations in the state of the system, via the combined analysis of the statistics of trajectory-to-trajectory fluctuations versus that of the fluctuations within single-trajectory wave functions. This analysis is clearly dependent on the specific unraveling scheme, and it appears at first sight to be of purely theoretical interest, given that the single-trajectory fluctuations are inaccessible experimentally, unless one is able to repeat the exact same trajectory (i.e., the same sequence of measurement records) multiple times. Nonetheless, the theoretical estimate of quantum fluctuations and correlations at the level of a specific unraveling scheme turns out to be much more relevant than what may at first appear, thanks to the link between this estimate and fundamental quantum coherence properties of the state of system $\hat{\rho}$.

A central quantity for the determination of quantum fluctuation and quantum correlation properties of a generic state $\hat{\rho}$ is the quantum Fisher information (QFI) related to an operator $\hat{A}$ [84,85], which is defined as

$$\text{QFI}(\hat{A}) = 2\sum_{lm}\frac{(\lambda_l - \lambda_m)^2}{\lambda_l + \lambda_m}|\langle l|\hat{A}|m\rangle|^2, \tag{16}$$

where $|l\rangle$ and $|m\rangle$ are eigenstates of $\hat{\rho}$ with respective eigenvalues λ_l and λ_m. The QFI represents the most important quantity in quantum interferometry, determining the ultimate sensitivity of state $\hat{\rho}$ to a unitary transformation generated by $\hat{U}(\theta) = e^{-i\theta\hat{A}}$. If $\hat{A}$ and $\hat{\rho}$ commute, such sensitivity is zero; hence, QFI ultimately probes the noncommutativity between $\hat{A}$ and $\hat{\rho}$, or, more explicitly, the amplitude of the quantum fluctuations of $\hat{A}$ in state $\hat{\rho}$.

QFI can also be used to probe entanglement in state $\hat{\rho}$. If $\hat{A}$ is a sum of local qubit observables, $\hat{A} = \sum_i \hat{A}_i$, the state sensitivity to the unitary transformation exceeds the standard quantum limit (SQL) $\Delta\theta = 1/\sqrt{N}$ of independent qubits only if the state is entangled [85,86], as detected by the fact that the QFI density exceeds unity: $\mathrm{QFI}(\hat{A})/N > 1$. In particular, the condition $\mathrm{QFI}(\hat{A})/N > p$ (with $p \in \mathbb{N}$) reveals that the system contains $(p+1)$-partite entanglement [87,88].

In quantum trajectory calculations we do not have direct access to QFI, which generically requires full knowledge of the density matrix. The stochastic unraveling of the density matrix evolution does offer a pure-state decomposition of state $\hat{\rho}$, but not its eigenstate decomposition [which is instead required by the definition of QFI, Eq. (16)]. Nonetheless, knowledge of a pure-state decomposition of the density matrix still gives access to an *upper* bound to QFI [54,89], in the form of the quantum fluctuations defined in Sec. III A 2, namely,

$$\mathrm{QFI}(\hat{A}) \leq 4\sum_n p_n \mathrm{Var}_{\psi_n}(\hat{A}) = 4F_q(\hat{A}). \tag{17}$$

Here p_n is the probability assigned to the pure state $|\psi_n\rangle$ by the quantum trajectory approach (e.g., in the steady state) and $\mathrm{Var}_{\psi_n}(\hat{A}) = \langle\psi_n|\hat{A}^2|\psi_n\rangle - \langle\psi_n|\hat{A}|\psi_n\rangle^2$ is the variance of $\hat{A}$ on the state of a single trajectory; hence, this expression is equivalent to the trajectory-sampling expression (11) for the quantum fluctuations in the limit $N_{\mathrm{traj}} \to \infty$. Inequality (17) becomes an equality only when extremizing F_q over all pure-state decompositions [54,89]. Given that the value of the upper bound in Eq. (17) is unraveling dependent, one could in principle find an optimal upper bound by exploring different unravelings, although we limit ourselves to heterodyne unraveling for this work.

The expression of the quantum fluctuations of $\hat{A}$ for the trajectory approach can be made more explicit by casting it in terms of quantum correlations C_q defined in Eq. (15):

$$F_q(\hat{A}) = \sum_{i,j} C_q(\hat{A}_i, \hat{A}_j). \tag{18}$$

Such a decomposition can be put in parallel with that of QFI for the macroscopic observable $\hat{A}$,

$$\mathrm{QFI}(A) = \sum_{ij} \mathcal{Q}_{ij}, \tag{19}$$

where $\mathcal{Q}_{ij} = \mathcal{Q}(\hat{A}_i, \hat{A}_j)$ is given by

$$\mathcal{Q}_{ij} = 2\sum_{lm} \frac{(\lambda_l - \lambda_m)^2}{\lambda_l + \lambda_m} \langle m|\hat{A}_i|l\rangle\langle l|\hat{A}_j|m\rangle, \tag{20}$$

the so-called quantum Fisher information matrix (QFIM; for the special case of commuting observables $[\hat{A}_i, \hat{A}_j] = 0$), and plays a central role in multiple phase estimation [90,91].

As we will see for the case of the dissipative XYZ model studied below, the unraveling-dependent quantum correlation function $C_q(\hat{A}_i, \hat{A}_j)$ has an exponentially decaying behavior as a function of distance in the steady states examined below $|C_q(\hat{A}_i, \hat{A}_j)| \sim \exp(-r_{ij}/\tilde{\ell}_Q)$, where $\tilde{\ell}_Q$ is an (unraveling-dependent) *quantum coherence length*, introduced for equilibrium mixed states in Ref. [92], and defining the characteristic spatial range of quantum correlations. Notably, this behavior is also generally expected for thermal states [92–94], as recently proven in Ref. [95]. It is reasonable to assume as well that the QFIM has a similar exponential decay, $|\mathcal{Q}_{ij}| \sim \exp(-r_{ij}/\ell_Q)$, where now the quantum coherence length ℓ_Q is an absolute property of state $\hat{\rho}$ and not of its stochastic sampling. The fact that the integral of C_q (given by F_q) is an upper bound to the integral of the QFIM (QFI itself) leads one to conclude that $\tilde{\ell}_Q \gtrsim \ell_Q$, namely, the spatial range of the unraveling-dependent quantum correlations C_q provides in practice an upper bound to that of the spatial range of the QFIM.

Hence, the above inequalities show that the quantum trajectory analysis of quantum fluctuations provides upper bounds to QFI and the quantum coherence length. One may expect the inequalities to be rather tight, since the unraveling corresponding to quantum state diffusion contains local jump operators only, and it is therefore likely to feature close-to-minimal entanglement in the trajectory states [96]. In Sec. IV E we also provide a lower bound to QFI, offered by the spin-squeezing parameter, allowing us to provide a definite quantitative estimate of QFI whenever the lower and upper bounds are close to each other.

B. Cumulant expansion and its truncation

In analogy with a classical probability distribution, the quantum state of a lattice system can either be specified by its expansion coefficients with respect to a Hilbert space basis or by the expectation values of a suitable set of single-site operators $\hat{X}_i$ (e.g., creation and annihilation operators for bosonic and fermionic systems, Pauli

matrices for spin systems). The moments of the local operators $\hat{X}_i$ are expectation values of the form $\langle \hat{X}_i^m \hat{X}_j^n \cdots \rangle$, where $k = m + n + \cdots$ is the order of the moment. Such moments can be conveniently expressed in terms of the multivariate *cumulants* $\langle \hat{X}_i^m \hat{X}_j^n \cdots \rangle_c$, which are recursively defined as [97,98]

$$\begin{aligned}
\langle \hat{X}_i \rangle &= \langle \hat{X}_i \rangle_c, \\
\langle \hat{X}_i \hat{X}_j \rangle &= \langle \hat{X}_i \hat{X}_j \rangle_c + \langle \hat{X}_i \rangle_c \langle \hat{X}_j \rangle_c, \\
\langle \hat{X}_i \hat{X}_j \hat{X}_k \rangle &= \langle \hat{X}_i \hat{X}_j \hat{X}_k \rangle_c + \langle \hat{X}_i \hat{X}_j \rangle_c \langle \hat{X}_k \rangle_c + \langle \hat{X}_i \hat{X}_k \rangle_c \langle \hat{X}_j \rangle_c \\
&\quad + \langle \hat{X}_j \hat{X}_k \rangle_c \langle \hat{X}_i \rangle_c + \langle \hat{X}_i \rangle_c \langle \hat{X}_j \rangle_c \langle \hat{X}_k \rangle_c,
\end{aligned} \tag{21}$$

and so on. A crucial insight justifying the use of a cumulant expansion is that, in typical situations of interest in physics—e.g., in the equilibrium state of many-particle systems—the value of the cumulants is expected to decrease with their order k. Therefore, a meaningful approximation scheme might consist in truncating the cumulant hierarchy to a given order k_c: in so doing, moments of order $k > k_c$ can be expressed in terms of the moments of order $1 \leq k \leq k_c$, and therefore the whole state is assumed to be described in terms of a finite set of moments, whose number grows polynomially with the system size as N^{k_c}. Approaches based on a truncation of the cumulant expansion for the moments of the fluctuations have been widely used in complex systems across physics; for example, in condensed matter and chemical systems [97,99–101], but also in quantum chromodynamics [102], cosmology [103], and even medical imaging [104]. In the context of driven-dissipative systems, cumulant approaches have been most commonly applied to bosonic systems and in particular on the level of the master equation [68,105–113]. Some recent work has shown the advantage of descriptions on the level of quantum trajectories for such systems instead, in particular at the Gaussian level [9,36,114]. Our goal here is to extend these methods to dissipative quantum spin lattices, exhibiting their potential to quantitatively describe dissipative phase transitions and the role of quantum fluctuations.

It must be noted that, while the truncation of the cumulant hierarchy often leads to insightful results, it is typically not variational, namely, it does not necessarily correspond to an existing ansatz for the quantum state. According to a well-known theorem of statistics proven by Marcinkiewicz [115], all classical probability density functions either have only nonvanishing $k \leq 2$ cumulants, or cumulants up to infinitely high order will be nonvanishing [116]. This has since been generalized to bosonic quantum states [117]. As a consequence of the Marcinkiewicz theorem, physical bosonic states have either only first-order cumulants (coherent states, $k_c = 1$), only first- and second-order cumulants (Gaussian states, $k_c = 2$), or nonzero cumulants to all orders. For the case of spin systems, we are not aware of an analog to the Marcinkiewicz theorem, although the existence of spin-to-boson mappings suggests that the limitations on the existence of physical truncations of the cumulant expansion valid for bosons may have similar repercussions on spins as well. We argue nonetheless that, even if the truncation to order k_c of the cumulant hierarchy did not correspond to any physical state for the quantum spins, its application to calculations amounts to an embedding of the physical problem of interest within a larger family of problems, a procedure which is rather common in physics. As an example, in the context of spin-to-boson mappings, quantum spins are mapped onto bosons with a constrained Hilbert space [118], but the necessity to release the constraints for the sake of feasible calculations embeds the quantum spin problem within a larger family of problems. The latter act is meaningful as long as the physical content of the theoretical predictions is not substantially altered by the embedding. In the following, we make this (falsifiable) assumption of the truncation of the cumulant expansion to order $k = k_c = 2$ for spin systems. We remark that throughout our study we have not encountered a single unphysical result justifying the need to revise this assumption, and have validated consistency with exact results where these could be obtained.

C. Truncated-cumulant equations for dissipative spin systems

In this work we focus our attention on spin-1/2 spins, in relation with current studies on ensembles of qubits coupled to each other and with an environment. For a spin-1/2 system, the local spin variables form a closed algebra, such that any product of spin operators acting on the same site can be written as a single spin variable. Therefore, the only local observables X_i of interest are the spin components $\hat{\sigma}_i^\alpha$, $\alpha = x, y, z$, taken to first power, whereas the nonlocal moments of interest are of the kind $\langle \hat{\sigma}_i^{\alpha_i} \hat{\sigma}_j^{\alpha_j} \hat{\sigma}_k^{\alpha_k} \cdots \rangle$ with $i \neq j \neq k$. As a consequence, a truncation of the cumulant hierarchy to order k_c implies that all k-point correlation functions with $k > k_c$ can be expressed in terms of k-point ones with $k \leq k_c$. In the following we adopt the truncation scheme of the cumulant expansions at the level of single trajectories, with $k_c = 2$. We note that some recent works have applied a similar truncation scheme to spin systems [111,112], but as an ansatz on the density matrix solving the master equation instead. In view of the discussion provided above on classical versus quantum correlations, we can state that the above-cited works truncate all correlations equally, whereas the approach we discuss here preserves classical fluctuations up to all orders, and only truncates the higher-order cumulants of quantum correlations. This is a much more flexible ansatz since, in analogy with the bosonic case, cumulants of order higher than $k = 2$ are preserved at the level of the

trajectory-to-trajectory fluctuations. We note that a truncation on quantum correlations is physically justified in a dissipative system, as high-order cumulants of quantum fluctuations may be expected to be strongly suppressed by decoherence [38], given that each site is assumed to interact with its own independent environment.

In the following we discuss the single-trajectory equations of motion for the moments of the spin fluctuations within the two truncation schemes with $k_c = 1$ (corresponding to the Gutzwiller mean-field ansatz for trajectories) and with $k_c = 2$, which is the truncation level we adopt for the rest of our work.

1. $k = 1$ truncation

When truncating the cumulant expansion to first-order cumulants, nonlocal quantum correlations are completely discarded, and the pure state along each trajectory corresponds to a factorized Gutzwiller ansatz [41]. We then obtain, from Eqs. (1), (2), and (7),

$$d\langle\hat{\sigma}^x_m\rangle = \Big(-\frac{\gamma}{2}\langle\hat{\sigma}^x_m\rangle + 2J_y \sum_{m'}\langle\hat{\sigma}^y_{m'}\rangle\langle\hat{\sigma}^z_m\rangle - 2J_z \sum_{m'}\langle\hat{\sigma}^z_{m'}\rangle\langle\hat{\sigma}^y_m\rangle\Big)dt + \sqrt{\frac{\gamma}{2}}(1 + \langle\hat{\sigma}^z_m\rangle - \langle\hat{\sigma}^x_m\rangle^2)dW^x_m + \sqrt{\frac{\gamma}{2}}\langle\hat{\sigma}^x_m\rangle\langle\hat{\sigma}^y_m\rangle dW^y_m, \tag{22}$$

$$d\langle\hat{\sigma}^y_m\rangle = \Big(-\frac{\gamma}{2}\langle\hat{\sigma}^y_m\rangle + 2J_z \sum_{m'}\langle\hat{\sigma}^z_{m'}\rangle\langle\hat{\sigma}^x_m\rangle - 2J_x \sum_{m'}\langle\hat{\sigma}^x_{m'}\rangle\langle\hat{\sigma}^z_m\rangle\Big)dt - \sqrt{\frac{\gamma}{2}}(1 + \langle\hat{\sigma}^z_m\rangle - \langle\hat{\sigma}^y_m\rangle^2)dW^y_m - \sqrt{\frac{\gamma}{2}}\langle\hat{\sigma}^x_m\rangle\langle\hat{\sigma}^y_m\rangle dW^x_m, \tag{23}$$

$$d\langle\hat{\sigma}^z_m\rangle = \Big(-\gamma(\langle\hat{\sigma}^z_m\rangle + 1) + 2J_x \sum_{m'}\langle\hat{\sigma}^x_{m'}\rangle\langle\hat{\sigma}^y_m\rangle - 2J_y \sum_{m'}\langle\hat{\sigma}^y_{m'}\rangle\langle\hat{\sigma}^x_m\rangle\Big)dt - \sqrt{\frac{\gamma}{2}}\langle\hat{\sigma}^x_m\rangle(1 + \langle\hat{\sigma}^z_m\rangle)dW^x_m + \sqrt{\frac{\gamma}{2}}\langle\hat{\sigma}^y_m\rangle(1 + \langle\hat{\sigma}^z_m\rangle)dW^y_m. \tag{24}$$

Note that these equations are expressed differently than those of Ref. [41], but are equivalent (modulo the choice of stochastic unraveling). We have also observed that they are numerically more efficient to integrate. When the noise terms are omitted in Eqs. (22)–(24), recovering the $k = 1$ truncation scheme at the level of the density matrix, these equations reduce to the mean-field equations described in Ref. [23].

In Appendix D we extend the $k = 1$ calculations of Ref. [41], and we provide a comprehensive finite-size scaling analysis of the dissipative paramagnetic-ferromagnetic phase transition exhibited by the $k = 1$ truncation scheme. This analysis shows that the $k = 1$ data are incompatible with the universality class of the 2D classical Ising, but have rather good agreement with the mean-field universality class; however, this picture is strongly altered by the inclusion of quantum correlations within the $k = 2$ truncation scheme, as we discuss further in Sec. IV D, which is in stark contrast with the treatment of classical correlations only.

2. $k = 2$ truncation

We now turn our attention to the more general $k > 1$ case, which allows one to account for quantum correlations in the dissipative dynamics. The derivation of the equations for the evolution follows the scheme outlined above, and in the $k = 2$ case it is detailed in Appendix A for heterodyne unraveling.

As already mentioned above, in the bosonic case only $k = 1, 2$ truncations correspond to variational states (coherent states and Gaussian states, respectively).

In the case of spin states, the situation is more intricate. The vanishing of cumulants of order larger than $k = 1$ is realized by Gutzwiller states (see Sec. III C 1). The absence of well-understood quantum spin states that display closure at the $k = 2$ level, however, does not mean that this truncation is without its merits in the description of physical systems.

It has actually been shown that almost all pure quantum states for $N = 3$ spins are in fact fully determined by knowledge of the two-spin density matrices [119]. This implies in turn that third-order cumulants must vanish exactly for these states. This result has been generalized to systems with $N > 3$ [120,121], where it has been proven that most quantum states are fully determined by knowledge of the reduced states involving only a fraction of its degrees of freedom—albeit generically a macroscopic fraction thereof. This suggests that truncated-cumulant hierarchies have physical relevance, even though the truncation to order $k_c = 2$ might not be realized exactly by a generic physical state for $N \gg 2$ spins.

The choice of $k = 2$ guarantees the ability to capture quantum correlation at the smallest computational cost—namely, that of tracking the evolution of two-point correlation functions, requiring a computational time of order $\mathcal{O}(N^2)$ for systems with short-range interactions. As noted above, these two-point quantum correlation functions are those most likely to survive decoherence and they are expected to dominate the critical behavior at true quantum phase transitions.

A technical remark is in order at this point. In the stochastic trajectory approach, the fluctuations of order $\sqrt{dt}$ result in equations that turn out to be numerically unstable. Stability is recovered however when the noise terms in the equations of motion for the second-order cumulants are dropped. The justification for omitting the noise terms in the dynamics of the second-order cumulants is detailed in Appendix B. There we show that the dynamics becomes more stable when the amplitude of the noise is reduced. Physically, this corresponds to a situation with detectors that have a limited efficiency, namely, that they only detect a portion of the photon signal emitted by the spins upon decaying. With these finite efficiencies, we see that the presence of noise on the second moments does not affect the results, and we can extrapolate the results to the (numerically unstable) trajectory limit with $\gamma_m = \gamma$. This observation therefore allows us to omit these noise terms on the second-order cumulants. Doing so, we observe very good agreement between the cumulant hierarchy and numerically exact results for small systems—as we detail below—further demonstrating the validity of this approach.

IV. RESULTS

In what follows we present the results for the dissipative *XYZ* model from our method obtained with the $k = 2$ cumulant truncation. In Secs. IV A–IV E, we focus our attention on the case $J_x = 0.9\gamma$ and $J_z = \gamma$; a full account of the phase diagram of the system will be provided in Sec. IV F. Note that, to obtain the expectation value of an operator $\hat{O}$ in the quantum trajectory formalism, we time evolve each quantum trajectory over a long enough period of time for it to reach the steady-state regime. Subsequently, we continue to time evolve and use this collected data to perform time averaging when calculating expectation values. Additionally, we average over multiple trajectory realizations.

A. The steady-state spin structure factor

We start by benchmarking the $k = 2$ truncation scheme, which amounts to tracking the evolution of one- and two-point correlators with ranges covering the entire lattice. To this end, we compare our results on the steady-state expectation values with the exact solutions of a 2×2, 3×3, and 4×4 lattice. For the two smaller lattices, we directly solve master equation (2), while the larger lattice is solved with a wave-function Monte Carlo approach based on the photon counting unraveling of Eqs. (4)–(6), which converges to the exact steady-state expectation values when averaging over a sufficient number of trajectories. The $\mathbb{Z}_2$ symmetry of the problem along the x and y axes prevents the appearance of a nonzero magnetization in the steady state; hence we resort to the steady-state (SS) spin structure factor to reveal the possible appearance of ferromagnetic order in the system. It is defined as

$$S^{\alpha\alpha}_{\mathrm{SS}}(\mathbf{k}) = \frac{1}{N^2}\sum_{i,j} e^{i\mathbf{k}\cdot\mathbf{r}_{ij}}\langle\hat{\sigma}^{\alpha}_i\hat{\sigma}^{\alpha}_j\rangle \tag{25}$$

with $\mathbf{r}_{ij} = \mathbf{r}_i - \mathbf{r}_j$. For the choice of $\mathbf{k} = 0$, a value of the structure factor not scaling with the system size signals the presence of long-range ferromagnetic order, while a value scaling to zero with system size (as N^{-1}) signals a paramagnetic phase. The results for the steady-state spin structure factor in the x direction are shown in Fig. 1(a) for values of $0 < J_y/\gamma < 2$. In the proximity of $J_y \approx \gamma$ we find excellent correspondence between our method and the exact solution. We refer the reader to Appendix C for additional data showing a comparison of the second and fourth moments in the x and y directions for the $k = 2$ trajectory method and the exact solution, once again exhibiting a rather remarkable correspondence.

Furthermore, as the system size increases, so does the region where the $k = 2$ results fall onto the exact solution. This can also be observed by studying the local maxima of the steady-state spin structure factor: for the maxima on both sides of $J_y = \gamma$, one can observe a decreasing difference with the exact solution as the system size is increased, suggesting that a result very close to the exact solution may in fact be recovered in the thermodynamical limit.

The agreement between the numerically exact solution and the $k = 2$ results is especially good in the region close to the paramagnetic-to-ferromagnetic phase transition, occurring in the vicinity of $J_y/\gamma = 1$ (as we will see in Sec. IV D), and in a way that is nearly independent of system size. This good correspondence for small system sizes gives confidence for the use of our method to study the critical properties around the transition. The very good agreement between the $k = 2$ results and the exact ones suggests that the cumulants that we discard (of order $k = 3$ and higher) are—as anticipated—significantly suppressed in the steady state as a result of the coupling to the environment.

Figure 1(b) exposes the significant improvement offered by the $k = 2$ results compared to the $k = 1$ ones throughout the range of parameters relevant for the physics discussed in this work. The same figure also shows that the application of the $k = 2$ truncation scheme at the level of single-trajectory wave functions, which stochastically

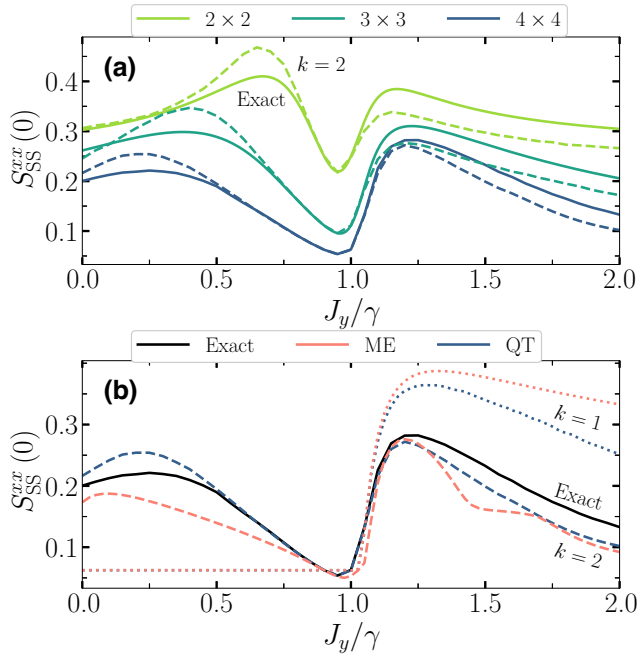

FIG. 1. (a) Steady-state spin structure factor for the $\hat{\sigma}^x$ spin components, $S^{xx}_{SS}(0)$, for a 2×2, 3×3, and 4×4 lattice as a function of J_y/γ ($J_x = 0.9\gamma$): dashed lines represent the results from the $k = 2$ truncation scheme, while solid lines are the exact steady-state solution, obtained by directly solving the master equation exactly for $N < 4$, and by sampling exactly calculated trajectories in the stochastic unraveling of the master equation for $N = 4$. The parameter region in which the $k = 2$ results overlap with the exact ones is seen to become progressively wider for larger system sizes. (b) Comparison of the same spin structure factor from different correlation-hierarchy methods, $k = 1$ (dotted lines) and $k = 2$ (dashed lines), for the 4×4 lattice, applied at the level of the master equation (ME) and at the level of quantum trajectories (QTs). For the data of both panels, and for all system sizes, the number of trajectories for the $k = 2$ calculations is given by $N_{\text{traj}} \approx 250$; the results are time averaged over the time interval $t\gamma \in [75; 150]$, corresponding to the stationary regime of the evolution.

sample the density matrix, delivers results that are in significantly better agreement with the exact solution than those obtained by applying the same truncation scheme for the full fluctuations, i.e., at the level of the master equation. This is especially visible in the vicinity of the transition at $J_y/\gamma \approx 1$.

In the ferromagnetic phase, long-range ferromagnetic order appears in the X-Y plane, but not necessarily along one of the coordinate axes, and it is therefore necessary to systematically search for the direction of maximal correlations. Such a direction is defined by the angle ϕ for which the $k = 0$ structure factor

$$S^{\phi\phi}_{SS}(0) = \cos^2\phi\, S^{xx}_{SS}(0) + \sin^2\phi\, S^{yy}_{SS}(0) + 2\sin\phi\cos\phi\, C^{xy}(0) \tag{26}$$

is maximal, where we have introduced the cross-correlation term

$$C^{xy}(\mathbf{k}) = \frac{1}{2N^2}\sum_{ij} e^{i\mathbf{k}\cdot\mathbf{r}_{ij}}\langle\hat{\sigma}^x_i\hat{\sigma}^y_j + \hat{\sigma}^y_i\hat{\sigma}^x_j\rangle. \tag{27}$$

Maximizing with respect to ϕ, one can easily obtain the following condition on the optimal angle:

$$\phi = \frac{1}{2}\tan^{-1}\left(\frac{2C^{xy}(0)}{S^{xx}_{SS}(0) - S^{yy}_{SS}(0)}\right) + \frac{p\pi}{2} \tag{28}$$

with $p \in \mathbb{Z}$. This condition allows for the extraction of angle ϕ that maximises the order parameter by simply calculating the three quantities $S^{xx}_{SS}(0)$, $S^{yy}_{SS}(0)$, and $C^{xy}(0)$. From this point onward we systematically focus on results for the optimal angle ϕ.

B. Paramagnetic phase with quantum properties

The qualitative correspondence of the $k = 2$ results allows us to investigate more closely the region $0 < J_y/\gamma < 1$. In this region the Gutzwiller approach (either at the level of the master equation or of the wave-function trajectories) predicts a featureless paramagnetic phase [23, 41], exhibiting a structure factor that is very close to zero for all system sizes. On the other hand, our $k = 2$ results show the existence of ferromagnetic correlations; the fact that they appear in this approach and not within the $k = 1$ scheme [44] indicates that they have a quantum origin, given that the account of quantum correlations is the main distinction between the two truncation schemes. An analysis of scaling with system size allows us to determine the fate of these quantum ferromagnetic correlations in the thermodynamic limit. In panel (a) of Fig. 2 we show the steady-state spin structure factor $S^{\phi\phi}_{SS}$ for various system sizes. It is clear that the maximum for the left peak decreases with increasing system size, but correlations persist for lattices of intermediate size. A finite-size scaling of the maximum, shown in panel (b) of Fig. 2, shows a power-law decrease proportional to $N^{-0.95}$. This signals that in fact the quantum ferromagnetic correlations are of short-range nature, as we show explicitly in the next section, and one recovers a paramagnetic phase as predicted by the Gutzwiller trajectory approach [44]. Nonetheless, as shown in Sec. IV E, the quantum nature of correlations present in this phase is not only underlined by the comparison with the Gutzwiller results, but it can be further characterized in terms of entanglement witnesses. Indeed, as we will see, substantial quantum correlations are accompanied by spin squeezing, offering a rather tight lower bound to the quantum Fisher information associated with the collective spin in some parameter regimes.

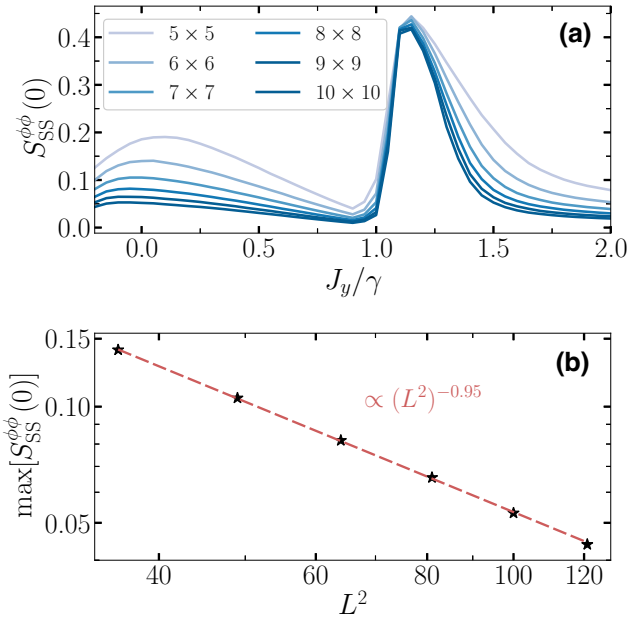

FIG. 2. (a) Steady-state spin structure factor for the $\hat{\sigma}^{\phi}$ spin components at the optimal angle, $S^{\phi\phi}_{\rm SS}(0)$, for lattices with dimensions $L = 5, \ldots, 10$, obtained via quantum trajectories within the $k = 2$ truncation scheme ($J_x = 0.9\gamma$). (b) Scaling of the local maximum of $S^{\phi\phi}_{\rm SS}(0)$ for $J_y/\gamma < 0.9$; the red line shows a power-law fit $\propto (L^2)^{-0.95}$. In both panels, the other simulation parameters are the same as for the $k = 2$ case presented in Fig. 1.

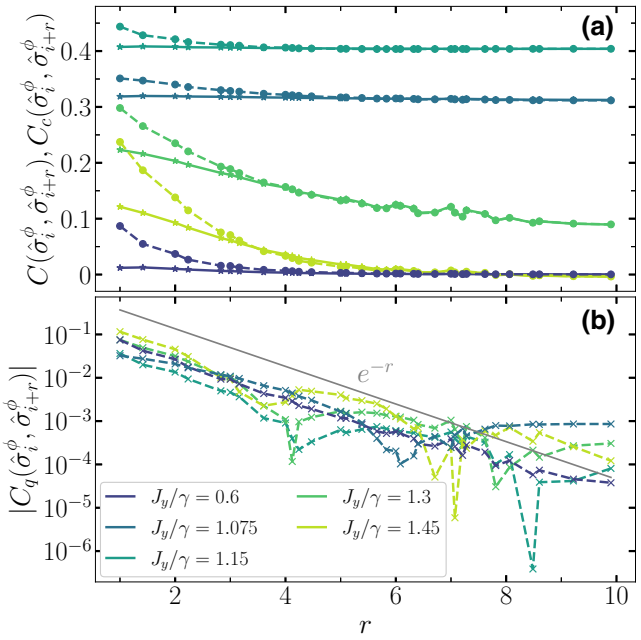

FIG. 3. (a) Total correlation function $C(\hat{\sigma}^{\phi}_i, \hat{\sigma}^{\phi}_{i+r}) = \langle \hat{\sigma}^{\phi}_i \hat{\sigma}^{\phi}_{i+r} \rangle$ for the optimal-angle spin components (dashed lines with filled circles), along with its classical part $C_c(\hat{\sigma}^{\phi}_i, \hat{\sigma}^{\phi}_{i+r})$ (solid lines with stars), for several values of J_y/γ at $J_x = 0.9\gamma$. (b) Quantum contribution to the correlations $C_q(\hat{\sigma}^{\phi}_i, \hat{\sigma}^{\phi}_{i+r})$ (dashed lines with crosses), compared with a reference exponential decay (solid line). In both panels, the data refer to a 14×14 lattice, and are obtained using $N_{\rm traj} = 128$ trajectories, with time averaging performed in the time interval $t\gamma \in [75; 150]$.

C. Long-range order and short-range quantum correlations

The most salient feature in Fig. 2(a) is the appearance of a strong peak in the structure factor, which is nearly size independent in the region $1 \lesssim J_y/\gamma \lesssim 1.25$, reflecting the appearance of long-range ferromagnetic order. The phase diagram therefore sees the succession of two transitions upon increasing J_y/γ: from paramagnetic to ferromagnetic around $J_y/\gamma \approx 1$ and from ferromagnetic back to paramagnetic around $J_y/\gamma \approx 1.25$. The critical behavior at these two transitions will be investigated in detail in Sec. IV D.

We now examine the steady-state correlation function $\langle \hat{\sigma}^{\phi}_i \hat{\sigma}^{\phi}_j \rangle$ for the optimal angle ϕ spin components, i.e., $\hat{\sigma}^{\phi}_i = \cos(\phi)\hat{\sigma}^x_i + \sin(\phi)\hat{\sigma}^y_i$. These correlations are shown in Fig. 3(a) for a 14×14 lattice and various values of J_y/γ using dashed lines with filled circles. In this figure we plot, along with the above-cited correlation function, the one associated with classical correlations, as defined in Eq. (14), namely, accounting only for trajectory-to-trajectory fluctuations of the single-trajectory average values $\langle \psi_n | \hat{\sigma}^{\phi}_i | \psi_n \rangle$. The differences between these data in turn give the quantum correlations as defined in Eq. (15).

We systematically observe for all values of J_y/γ that classical correlations and total correlations tend to coincide at long distances, indicating that the paramagnetic-to-ferromagnetic and ferromagnetic-to-paramagnetic transitions in the system are fundamentally driven by classical fluctuations—this conclusion will also be corroborated in the Sec. IV D with the analysis of the universality class of the transition. Nonetheless, we clearly observe the presence of very pronounced *short-range* quantum correlations, in that classical and total correlations significantly deviate from each other at shorter distances. More precisely, as shown in Fig. 3(b), we observe exponentially decaying quantum correlations exhibiting a finite quantum coherence length $\tilde{\ell}_Q$, as defined in Sec. III A 3. Remarkably, we observe $\tilde{\ell}_Q \approx 1$, the lattice constant, across all parameter values. The ability of the method to tackle rather large lattices allows us to describe the full spatial structure of quantum correlations. Their short-ranged nature may erroneously suggest that one may ignore them altogether (as done by Gutzwiller trajectory approaches, or their cluster extensions for distances beyond the cluster size) and that this will not bear any consequence on the study of the critical behavior of the system—which, by definition, involves only long-range correlations. In fact, we see in the next section that taking quantum correlations

into account properly has profound consequences for the critical behavior, in spite of its seemingly classical nature.

D. Phase transitions and universal behavior

We now turn to a systematic finite-size scaling analysis of the two transitions appearing in the system: the paramagnetic-to-ferromagnetic transition for $J_y/\gamma \approx 1$ and the transition to reentrant paramagnetism for $J_y/\gamma \approx 1.25$. While the presence of the first phase transition is well established, the second one is debated, and in fact even proposed to be a smooth crossover [42]. In particular, a difficult aspect for this transition is that it occurs in a regime in which the steady state has high entropy, posing a challenge to all density matrix methods that are limited in the entropy content of the state [32,40]. We argue that, *a priori*, our method should be able to capture the proper critical behavior regardless of whether it is driven by classical or quantum fluctuations.

1. Structure factor

In analogy with equilibrium thermal phase transitions, we assume that the behavior of the system exhibits scale invariance at a dissipative phase transition, so that the singular part of all thermodynamic quantities in turn exhibits a scaling behavior, governed by critical exponents. As a consequence of such scaling behavior, the structure factor at the optimal angle ϕ is expected to exhibit the following scaling behavior in finite-size systems:

$$S^{\phi\phi}_{\mathrm{SS}}(0) = L^{-2\beta/\nu} F(|J_y - J_{y,c}|L^{1/\nu}). \tag{29}$$

Here $J_{y,c}$ is the critical value for our control parameter J_y, L is the linear system size, F is a universal scaling function, and β, ν are universal critical exponents. In order to extract the three parameters $J_{y,c}$, β, and ν from a finite-size scaling analysis of our $k = 2$ results, we should adjust the values of the parameters so that the curves for $S^{\phi\phi}_{\mathrm{SS}}(0)L^{2\beta/\nu}$ plotted as a function of $|J_y - J_{y,c}|L^{1/\nu}$ for different system sizes collapse together, reconstructing the universal scaling function F. Reducing the number of fitting parameters, we start off with an educated guess, and immediately observe the consistence of our results with the 2D Ising universality class. Indeed, the insight gained by the analysis of correlations in the previous section showed us that long-range correlations in the system are of classical origin, so that we should expect the transitions (from paramagnetic to ferromagnetic and back) to be of a classical nature, and compatible with the $\mathbb{Z}_2$ symmetry of the system, its two-dimensional nature, and the short-range nature of its couplings. These characteristics suggest the 2D classical Ising universality class as a natural candidate for our transition, inviting us to fix the critical exponents to the corresponding values $\beta = 1/8$ and $\nu = 1$. Therefore, the only parameter to be adjusted remains $J_{y,c}$.

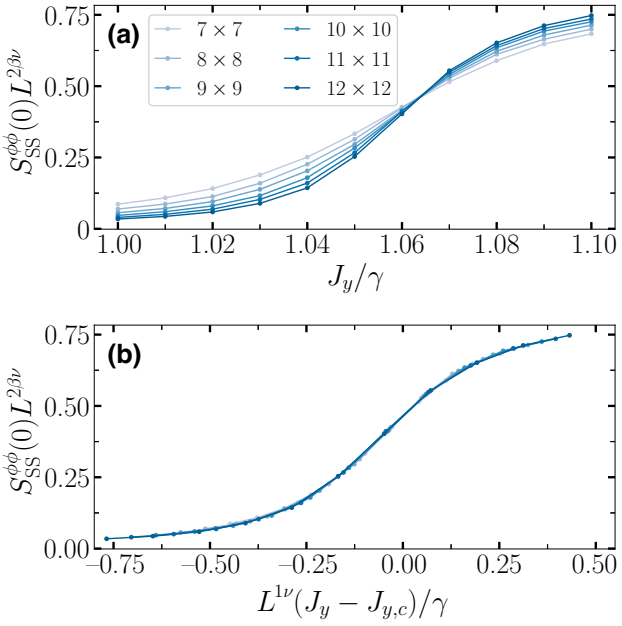

FIG. 4. (a) Rescaled structure factor $S^{\phi\phi}_{\mathrm{SS}}(0)L^{2\beta/\nu}$ at the paramagnetic-to-ferromagnetic transition for $J_x = 0.9\gamma$, using 2D Ising exponents ($\nu = 1$ and $\beta = \frac{1}{8}$). (b) Full scaling plot, using $J_{y,c} \approx 1.064$ as the critical point. For all system sizes, the number of trajectories is given by $N_{\mathrm{traj}} \approx 768$, and time averaging is performed in the interval $t\gamma \in [75; 150]$.

The value of $J_{y,c}$ can be extracted as the crossing point J_y between curves of the rescaled structure factor $S^{\phi\phi}_{\mathrm{SS}}(0)L^{2\beta/\nu}$ for different system sizes. Our results show a crossing at $J_y/\gamma \approx 1.064$ [Fig. 4(a)] for the first transition, and at $J_y/\gamma \approx 1.24$ [Fig. 5(a)] for the second one. The proof that the transition belongs to the classical 2D Ising universality class comes when plotting the rescaled structure factor as a function of the rescaled distance to the critical point $|J_y - J_{y,c}|L^{1/\nu}$ with $\nu = 1$: Figs. 4(b) and 5(b) show an excellent collapse for the first transition, and a very good one for the second transition when looking at the largest lattices (from 9×9 to 12×12). The apparently imperfect collapse at the second transition for smaller system sizes is clearly due to finite-size effects, as already visible in Fig. 5(a), in which the crossing point of the curves stabilizes only starting from the 9×9 lattice, as can be seen in the inset of Fig. 5(a). The above results therefore provide conclusive evidence for the existence of two transitions, both belonging to the 2D classical Ising universality class.

As discussed in Appendix D, a similar scaling analysis shows that the results obtained within the $k = 1$ (Gutzwiller) scheme are *not* compatible with a 2D Ising transition, nor with a mean-field one—in fact, we can obtain a scaling collapse of our $k = 1$ data only for effective critical exponents that do not correspond to any

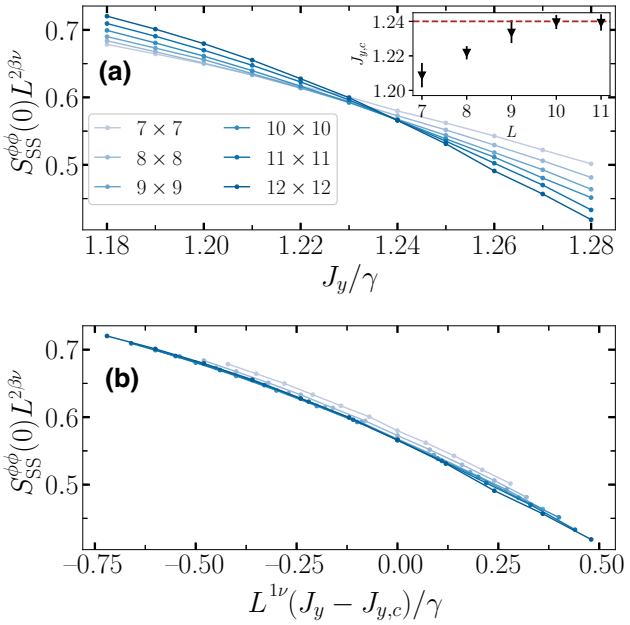

FIG. 5. (a) Rescaled structure factor $S^{\phi\phi}_{SS}(0)L^{2\beta/\nu}$ at the ferromagnetic-to-paramagnetic transition for $J_x = 0.9\gamma$, using 2D Ising exponents ($\nu = 1$ and $\beta = \frac{1}{8}$). Inset: crossing points $J_{y,c}$ of the curves associated with sizes L and $L+1$. (b) Full scaling plot, using $J_{y,c} \approx 1.24$ as the critical point. For all system sizes, the number of trajectories is given by $N_{\text{traj}} \approx 1408$ for $L = 7, 8, 9$, $N_{\text{traj}} \approx 1920$ for $L = 10, 11$, and $N_{\text{traj}} \approx 1792$ for $L = 12$, and time averaging is performed in the interval $t\gamma \in [75; 150]$.

equilibrium universality class known to us. This result is rather surprising, in view of the fact that one would expect the $k = 1$ approach to capture classical fluctuations at the dissipative transition, and that such fluctuations are expected to govern the critical behavior. From this observation we conclude that short-range quantum correlations, included in the $k = 2$ approach, are essential in determining the universality class, even though the long-range correlations that emerge at criticality are of classical origin. We can partially attribute this to the fact that the diffusion constants in the $k = 1$ model become zero in the paramagnetic phase so that no noise is left there. This aspect is rather surprising, but it shows that dissipative phase transitions often defy the intuition for critical phenomena that one may have developed in the context of equilibrium systems. Indeed, we can put this observation in parallel with the (equally surprising) one that cluster mean-field approaches [39], only including short-range correlations, radically change the prediction for the phase diagram of our system of interest compared with the standard mean-field approach [23]. In both cases, one observes that the proper account of fluctuations at short scales in dissipative quantum systems can have significant consequences on the long-wavelength properties.

2. Derivative of the transverse magnetization

The steady state of the dissipative *XYZ* model at study is generally characterized by the presence of a net magnetization $m^z = \langle \hat{J}^z \rangle / N = N^{-1} \sum_i \langle \hat{\sigma}_i^z \rangle$ along the z axis—which is induced by the fact that dissipation in the form of spontaneous decay favors the spin to point downwards along this axis. The m^z magnetization takes the value of -1 at the U(1) symmetry point of the model ($J_x = J_y$), at which the steady state is fully polarized along $-z$ by the dissipation given that M^z is a good quantum number. But it decreases (in absolute value) with respect to is saturation value as soon as $J_y \neq J_x$ because of quantum effects, given that Hamiltonian $\hat{H}$ ceases to commute with $\hat{J}^z$. Upon increasing the value of J^y/γ at fixed J^x/γ, the m^z curve clearly exhibits two size-dependent anomalies, corresponding to the two transitions of the system, as shown in Fig. 6(a): a sharp decrease (in absolute value) at the first (paramagnetic-to-ferromagnetic) transition and a successive upturn (again in absolute value) at the second (ferromagnetic-to-paramagnetic) transition. These features are best captured by taking the derivative of the magnetization with respect to the control parameter of the transition $\gamma\, dm^z/dJ_y$: this derivative—shown in Fig. 6(b)—exhibits two sharp size-dependent features, namely, a sharp growing peak and an equally sharp growing dip. Tracking the size dependence of the height of the peak (at the paramagnetic-to-ferromagnetic transition) we observe that it is compatible with a logarithmic growth $\gamma (dm^z/dJ_y)_{\text{peak}} \approx A + B \log L$ [Fig. 6(c)]. A similar behavior is observed as well for the dip in the derivative at the second transition, as shown in Fig. 6(d). A logarithmic growth is to be expected according to the 2D Ising universality class: indeed, a similar logarithmic divergence of the derivative of the transverse magnetization with respect to the control parameter of the transition (the temperature, in this case) is observed at the thermal transition of the 2D Ising model in a transverse field, and, as discussed in Appendix E from the scaling form of the free energy, it can be proven to be equivalent to the well-known logarithmic divergence of the specific heat peak at the 2D Ising transition [122]. Therefore, this result corroborates further the adherence of the two transitions of the system to the 2D Ising universality class, as well as the ability of the $k = 2$ truncation scheme approach to dissipative phase transitions to accurately reconstruct the multiple facets of critical behavior.

E. Bounds on the quantum Fisher information

1. Spin squeezing as an entanglement witness

In Sec. IV C we already ascertained the existence of short-range quantum correlations along each stochastic trajectory. Nonetheless, this result is strongly dependent on the properties of the trajectory wave functions, and

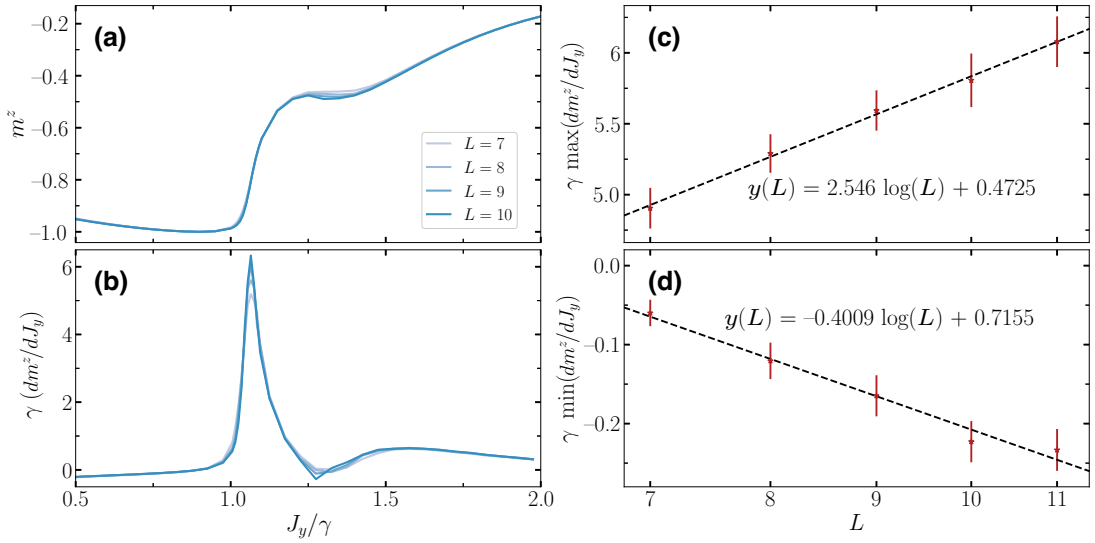

FIG. 6. (a) Dissipation-induced transverse magnetization m^z as a function of J_y for $J_x = 0.9\gamma$ and different system sizes. (b) Derivative of the transverse magnetization $\gamma dm^z/dJ_y$, showing two clear anomalies at the two transitions of the system. (c) Scaling of the peak value of $\gamma dm^z/dJ_y$ with system size (around $J_y/\gamma \approx 1$). (d) Scaling of $\gamma dm^z/dJ_y$ at the minimum value (around $J_y/\gamma \approx 1.25$). In panels (c) and (d) the dashed line is a logarithmic fit to the data. The numbers of trajectories used in (a) and (b) are $N_{\rm traj} \approx 250$ and $N_{\rm traj} \approx 750$ in the region close to $J_y \approx 1.05$. In panel (c) the number of trajectories range from $N_{\rm traj} \approx 27\,000$ to $N_{\rm traj} \approx 15\,000$ and in panel (d) from $N_{\rm traj} \approx 70\,000$ to $N_{\rm traj} \approx 35\,000$ (depending on the lattice dimension). For each trajectory, time averaging is performed in the interval $t\gamma \in [75; 150]$.

it could in principle be interpreted as depending on the specific unraveling that we are considering. Nonetheless, as already discussed in Sec. III A 3, the integral of the (unraveling-dependent) quantum correlations

$$F_q(\hat{J}^\phi) = \sum_{i,j} \Big[\cos^2\phi\, C_q(\hat{\sigma}_i^x, \hat{\sigma}_j^x) + \sin^2\phi\, C_q(\hat{\sigma}_i^y, \hat{\sigma}_j^y) + \frac{1}{2}\sin(2\phi)\,(C_q(\hat{\sigma}_i^x, \hat{\sigma}_j^y) + C_q(\hat{\sigma}_i^y, \hat{\sigma}_j^x)) \Big] \tag{30}$$

provides an upper bound to QFI of the collective spin component along the optimal angle $\hat{J}^\phi = \sum_i \sigma_i^\phi$, QFI$(\hat{J}^\phi)$, and the spatial decay of quantum correlations defines a similar bound to the spatial decay of the QFIM. Here we discuss how our calculations can in turn access a *lower* bound to QFI$(\hat{J}^\phi)$, therefore allowing for a quantitative estimate of its value.

The quantity of interest is related to the *spin-squeezing parameter*, which probes the structure of the uncertainty on the orientation of the collective spin $\hat{J}^\alpha = \sum_i \sigma_i^\alpha$ ($\alpha = x, y, z$). We observe that the state of the system is magnetically polarized along the negative z direction for the spins because of spontaneous decay—namely, it develops a finite value for $\langle J^z \rangle$ in the steady state. Moreover, at the transition the uncertainty on the collective spin component at the optimal angle ϕ, $\hat{J}^\phi = \cos\phi \hat{J}^x + \sin\phi \hat{J}^y$, develops anomalous critical fluctuations; if these fluctuations have an enhanced quantum component then one can expect that anomalously small fluctuations are developed by the perpendicular collective spin component $J^{\phi_\perp}$, as observed at Ising quantum critical points [123]. Under these circumstances, entanglement can be effectively detected in the form of squeezing, namely, by the fact that the squeezing parameter [124]

$$\xi_R^2 = \frac{N\,\mathrm{Var}(\hat{J}^{\phi_\perp})}{\langle \hat{J}^z \rangle^2} \tag{31}$$

becomes smaller than unity, or, equivalently, $\xi_R^{-2} > 1$. This condition is enough to show that the state is not separable [125].

The inverse of the squeezing parameter inherits its entanglement witnessing properties (discussed in Sec. III A 3) from the fact that it is a lower bound to QFI associated with the most strongly fluctuating collective spin component, QFI$(\hat{J}^\phi)$. Indeed, the inverse squeezing parameter represents a *lower* bound to the QFI density, $\xi_R^{-2} \leq \mathrm{QFI}(\hat{J}^\phi)/N$ [85], as it offers the gain in metrological precision (compared to the SQL) using a specific measurement protocol (Ramsey interferometry [124]). Therefore, the entanglement witnessing properties of QFI are directly transferred to the inverse spin-squeezing parameter.

2. Results

Our estimate of QFI of the steady state proceeds then by exploiting the inequality chain

$$\xi_R^{-2} \leq \frac{\mathrm{QFI}(\hat{J}^\phi)}{N} \leq \frac{4F_q(\hat{J}^\phi)}{N}, \tag{32}$$

and by explicitly calculating the two bounds. Figure 7(a) shows the inverse squeezing parameter (solid lines) for different system sizes as a function of J_y/γ scanning across the two dissipative phase transitions of the system. We observe that squeezing (namely, the condition $\xi_R^{-2} > 1$) is massively present in the phase diagram of the system: in particular, squeezing accompanies the first paramagnetic-to-ferromagnetic transition at $J_y/\gamma \approx 1$, and, most prominently, it is present across a wide region of the paramagnetic phase for $J_y/\gamma < 1$, which, as already pointed out in Sec. IV B, is accompanied by pronounced quantum correlations. The cusp singularity of squeezing for $J_y/\gamma = J_x/\gamma = 0.9$ marks the fact that the steady state at this symmetry point is the factorized pure state $|\downarrow\downarrow\cdots\downarrow\rangle$. The fact that squeezing is nearly independent of the system size is a reflection of the fact that quantum correlations are short ranged, as already explicitly shown in Sec. IV C. At the same time, squeezing is absent at the second transition for $J_y/\gamma \approx 1.2$. The striking difference between the behavior at small J_y/γ versus the behavior at larger J_y/γ is certainly a consequence of the fact that the regime at larger J_y/γ exhibits much larger entropies [40], so that quantum coherence effects are expected to be suppressed.

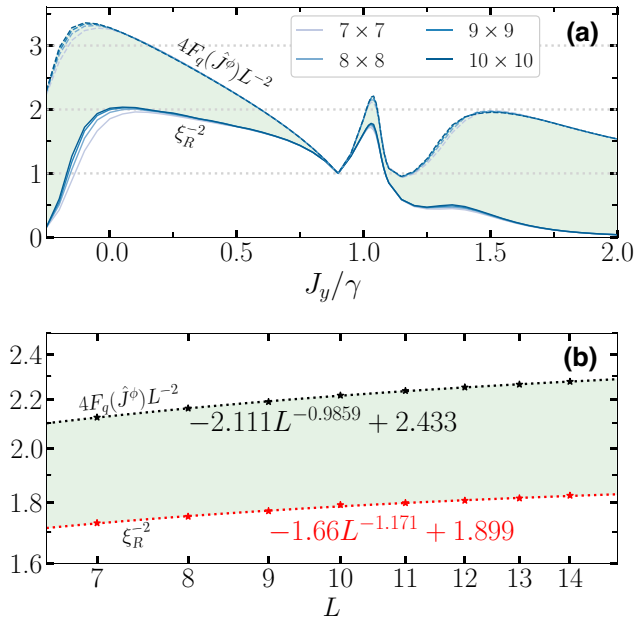

FIG. 7. (a) Inverse spin-squeezing parameter ξ_R^{-2} (lower solid curves) and $4F_q(\hat{J}^\phi)$ (upper dashed curves) as a function of J_y/γ ($J_x/\gamma = 0.9$) for different system sizes. The two sets of curves provide a lower and upper bound to $\mathrm{QFI}(\hat{J}^\phi)$, respectively [see Eq. (32)], whose value is therefore enclosed within the green-shaded area (for a 10×10 lattice). For all system sizes, the number of trajectories is given by $N_{\mathrm{traj}} \approx 770$, and time averaging is performed in the time interval $t\gamma \in [75; 150]$. (b) Scaling of the maximum of ξ_R^{-2} and of $4F_q(\hat{J}^\phi)$ near the paramagnetic-to-ferromagnetic transition ($J_y \approx 1.064\gamma$).

While the presence of squeezing is conclusive proof for the entangled nature of the state, its absence does not allow one to draw any conclusion about the nature of the state, since entanglement may still be witnessed by another criterion. Such a criterion could be offered by the QFI density exceeding unity, which is more effective than the squeezing criterion as, by construction, it detects all metrologically useful forms of entanglement, irrespective of the measurement protocol used to exploit it. In Fig. 7(a) we show both bounds for the QFI density appearing in Eq. (32), as they evolve across the two phase transitions. There we observe that the inequality chain becomes tight in the vicinity of the factorization point $J_y/\gamma = 0.9$ and of the first transition, revealing that squeezing is in fact the nearly optimal metrological resource of the steady state of the system, ensuring a sensitivity of the state to rotations that exceeds the SQL. On the other hand, the bound becomes looser for smaller values of J_y/γ as well as larger ones. This may mean that the heterodyne unraveling is simply far from that minimizing the quantum fluctuations on pure state decompositions in Eq. (17), or that metrologically useful entanglement exists in these regimes instead, but in forms different from (or superior to) spin squeezing. The conclusive aspect of our analysis in these regimes is that the upper bound on the QFI density, $4F_q(\hat{J}^\phi)$, does *not* appear to scale with system size, which implies that the QFI density itself cannot scale either: this is yet another consequence of the short-range nature of quantum correlations, pointed out in Sec. IV C. To corroborate this observation, an analysis of the scaling near the paramagnetic-to-ferromagnetic transition where $J_y \approx \gamma$ is shown in Fig. 7(b). Both the lower and upper bounds on the QFI density converge to finite values in the thermodynamic limit, approximately 1.9 and approximately 2.4, respectively, as indicated by their respective fits. Hence, the QFI density, albeit not scalable, is predicted to witness entanglement in the infinite-size limit.

F. Phase diagram: total and quantum correlations

We conclude this section with an overview of total and quantum correlations across the phase diagram of the system at fixed $J_z/\gamma = 1$, and for variable J_x/γ and J_y/γ. First of all, let us remark that the phase diagram is symmetric under the exchange $J_x \leftrightarrow J_y$, namely, it is mirror symmetric around the $J_x = J_y$ axis. Moreover, there is a mirror symmetry when the signs of both J_x and J_y are switched, and concomitantly ferromagnetic phases in the x-y plane are mapped to antiferromagnetic ones [23]. This latter symmetry reflects the fact that the canonical transformation $\sigma_i^{x(y)} \to (-1)^i \sigma_i^{x(y)}$, corresponding to a π rotation of one of the two sublattices of the square lattice, leaves the dissipation term unchanged in the GSKL equation; it

therefore establishes a correspondence between the steady states of the system with couplings J_x, J_y and that of the system with couplings $-J_x, -J_y$.

1. Structure factor

Figure 8 shows the evolution of total correlations throughout the phase diagram, as captured by the maximum of the structure factors at the optimal angle ϕ, namely, the maximum between $S^{\phi\phi}_{\rm SS}(\mathbf{k}=0)$ (characterizing the ferromagnetic phase) and $S^{\phi\phi}_{\rm SS}(\mathbf{k}=(\pi,\pi))$ (characterizing the antiferromagnetic phase). The results shown in Fig. 8 are obtained on a 6×6 lattice: this system size is smaller than those used to obtain the results presented above, yet sufficient to capture the overall shape of the phase diagram. We can clearly observe two ferromagnetic and two antiferromagnetic islands, surrounded by paramagnetic regions. The transitions from paramagnetic behavior to ferro/antiferromagnetic order appear rather sharp in the vicinity of the symmetry axis $J_x = J_y$, but much smoother away from it, revealing that finite-size effects are more pronounced in those ranges of parameters; as a consequence, one may erroneously deduce from the study of a finite system that the (anti)ferromagnetic behavior persists for much larger values of $|J_y|$ or $|J_x|$, or that the paramagnetic phase does not in fact reappear at all when moving far away from the symmetry axis, as predicted at the mean-field level [23]. Yet the existence of a true (anti)ferromagnetic-paramagnetic transition at large J_y (or J_x) was firmly established by our results of Sec. IV D.

The ferromagnetic (FM) and antiferromagnetic (AFM) islands are connected by an arc-shaped line of maxima in the structure factor. In fact, a cut through one of these arcs already appeared in Fig. 2 around $J_y = 0$. The finite size scaling in Fig. 2(b) showed that the structure factor tends to zero in the thermodynamic limit, and that the origin of the local maximum of the structure factor is an enhancement of quantum fluctuations. This enhancement corresponds to a crossover between a strongly polarized paramagnetic phase ($m^z \gtrsim -1$) and a much more weakly polarized paramagnetic phase ($|m^z| \ll 1$).

Our analysis does not consider any spin-density-wave phase, which is instead predicted by the mean-field analysis [23] in a small region of the diagram at high and slightly unequal J_x, J_y. The reason is that its appearance in a finite system is restricted by commensurability of the period with the lattice constant and system length.

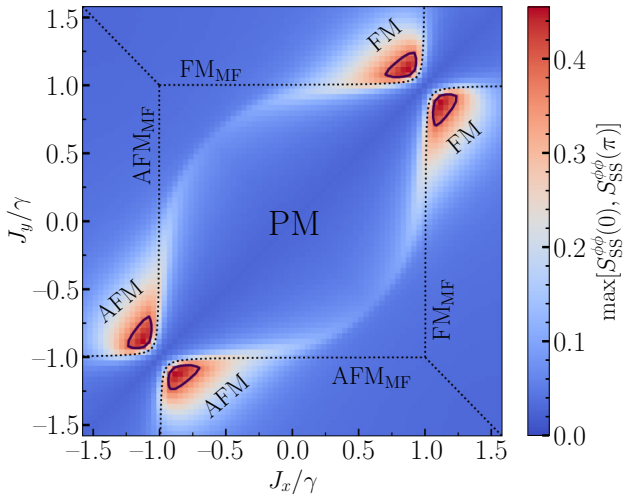

FIG. 8. Maximum of the structure factor, $\max[S^{\phi\phi}_{\rm SS}(0), S^{\phi\phi}_{\rm SS}(\pi,\pi)]$, for a 6×6 lattice with $J_z = \gamma$. The black dotted lines show the mean-field predictions (indicated by a MF subscript) for the boundaries of the FM and AFM phases. The solid black lines show the contour line where the (maximal) structure factor is equal to its value at the critical point $(J_x, J_{y,c})/\gamma = (0.9, 1.24)/\gamma$, repeated three times by reflection symmetry around the $J_x = J_y$ axis and around the $J_x = -J_y$ axis. Each data point is obtained with $N_{\rm traj} \leq 320$ trajectories and time averaging is performed in the time interval $t\gamma \in [50, 150]$.

2. Spin squeezing and the upper bound to the quantum Fisher information

As for the behavior of quantum correlations across the phase diagram, Fig. 9 shows the evolution of the inverse squeezing parameter $\max(\xi^{-2}_{R,\rm FM}, \xi^{-2}_{R,\rm AFM})$, where $\xi^2_{R,\rm FM}$ is the squeezing parameter defined in Eq. (31), while $\xi^2_{R,\rm AFM}$ corresponds to the squeezing parameter defined with the variance of the staggered magnetization

$$\xi^2_{R,\rm AFM} = \frac{N\,\mathrm{Var}(J^{\phi_\perp}_{\rm st})}{\langle J^z\rangle^2}, \tag{33}$$

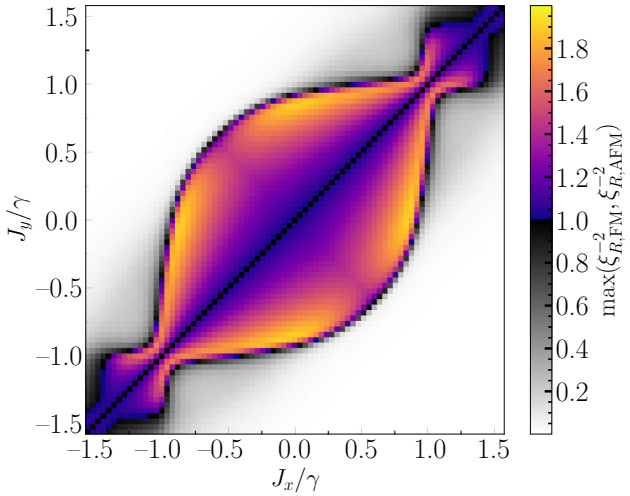

FIG. 9. Maximum of the inverse of the spin-squeezing parameter ξ_R^{-2} for the collective spin with uniform (FM) or staggered (AFM) collective spin in the x-y plane. All simulation parameters are as in Fig. 8.

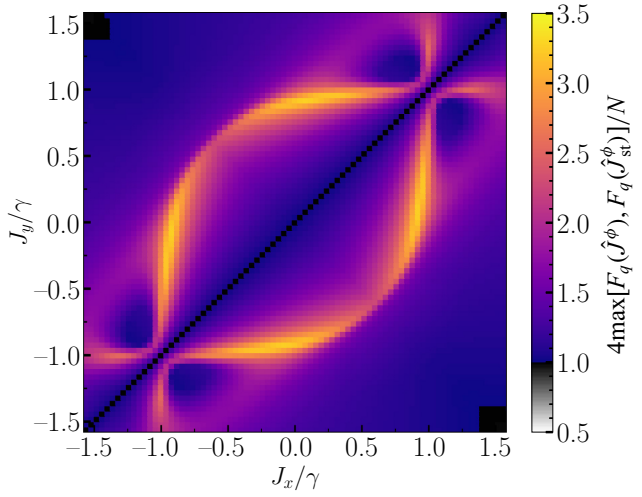

FIG. 10. Maximum upper bound to QFI of collective spin components, $4\max[F_q(\hat{J}^\phi), F_q(\hat{J}^\phi_{\rm st})]/N$. All simulation parameters are as in Fig. 8.

where we have introduced the staggered total spin $\hat{J}^{\phi_\perp}_{\rm st} = \sum_i (-1)^i \hat{\sigma}_i^{\phi_\perp}$ at angle $\phi_\perp$ perpendicular to the optimal one. On the other hand, Fig. 10 shows the evolution of the unraveling-dependent upper bound $4\max[F_q(\hat{J}^\phi), F_q(\hat{J}^\phi_{\rm st})]/N$, where we have introduced the staggered total spin $\hat{J}^\phi_{\rm st}$ at the optimal angle ϕ. The maximization procedure used for both figures allows us to correctly capture the amount of quantum correlations in the ferromagnetic regime as well as antiferromagnetic one of the phase diagram.

We observe that squeezing is a characteristic of the whole low-entropy paramagnetic regime enclosed between the $J_x = J_y$ symmetry axis and the arc-shaped lines of maxima of the structure factor. In particular, it becomes very pronounced along the boundaries of the (A)FM islands that are closest to the $J_x = J_y$ symmetry axis, and especially so for $J_y/\gamma \lesssim 1$ and $J_x/\gamma \ll 1$, and symmetrically for $J_x/\gamma \lesssim 1$ and $J_y/\gamma \ll 1$, and all along the arcs connecting the FM and AFM islands.

The same regions are also highlighted as being those potentially hosting the strongest quantum correlations when looking at the behavior of the upper bound $4F_q(\hat{J}^\phi)$ (somewhat surprising given that this phase is described reasonably well with mean-field theory), with the possibility that the reentrant paramagnetic phase at large distance from the symmetry axis also be quantum correlated (albeit not squeezed). On the other hand, both ξ_R^{-2} and $4F_q(\hat{J}^\phi)$ single out the ferromagnetic and antiferromagnetic phases as being those hosting the weakest quantum correlations in their respective parameter ranges.

V. CONCLUSIONS

In this work, we have introduced a new technique for the theoretical study of driven-dissipative many-body spin systems. Our method is based on the combination of the quantum trajectory approach to dissipative evolutions and of a description of the state along each trajectory based on one- and two-point spin-spin quantum correlation functions only, following a truncation scheme of the cumulant hierarchy for the pure states along each trajectory. Our approach is able to account for both classical and quantum fluctuations at all length scales, and it uniquely makes a simplifying assumption on the statistics of quantum fluctuations along each trajectory. Such an assumption is crucial to limit the computational cost of our approach to an $\mathcal{O}(N^2)$ polynomial scaling with N quantum spins (for short-range interactions), making large system sizes ($N \gtrsim 200$) accessible.

We have applied our method to the dissipative two-dimensional XYZ model, a paradigmatic nonequilibrium system that shows a rich and debated phase diagram. In particular, we find that the reentrant phase transition from the ferromagnetic to the paramagnetic state upon increasing the coupling of one of the spin components is a true phase transition rather than a crossover. Finite-size scaling of the order-parameter fluctuations conclusively shows that the critical behavior near both transitions belongs to the classical 2D Ising universality class. The classical nature of criticality at the dissipative phase transitions of the model is further supported by our analysis of classical versus quantum correlations associated with the trajectory unraveling. We find that quantum correlations are always short ranged, even close to the phase transition, so that the critical behavior is systematically dominated by the classical fluctuations between the different trajectories. Nonetheless, accounting for short-ranged quantum correlations appears to have crucial repercussions on the ensuing critical behavior: indeed, neglecting quantum correlations altogether (as in the Gutzwiller-state trajectories) leads to critical behavior incompatible with the 2D Ising. In fact, the critcal behaviour is rather difficult to analyze in light of known universality classes. The latter holds even if short-range quantum correlations restricted to "clusters" are considered. Moreover, quantum correlations, albeit short ranged, are still associated with certifiable entanglement related to spin squeezing. This form of entanglement is *enhanced* at the paramagnetic-ferromagnetic transition, showing that the competition between the coherent Hamiltonian dynamics and the incoherent coupling to a bath can in fact induce quantum entanglement in the steady state when tuned in the vicinity of a dissipative critical point. Surprisingly, we also predict significant entanglement in the paramagnetic phase, specifically at the crossover region that replaces the mean-field paramagnetic-to-(anti)ferromagnetic phase transitions. We note that we have mapped the phase diagram for fixed J_z/γ, but changing this parameter is expected to mostly lead to a shift of the position of the phases, while leaving the overall features of the phase diagram unchanged.

A possible exception could be the limit $J_z/\gamma \to 0$, where a staggered XY phase is predicted to appear by mean-field theory [23]; yet, a more extensive study of the latter phase [49] indicates that it may be unstable to fluctuations beyond the mean-field approximation. Our simulations did not include pure dephasing jumps (Lindblad operators of the form $\hat{\sigma}_z$) either, which might also be an additional effect of the environment [23]. However, since we already found that the critical behavior is dominated by classical fluctuations, we do not expect the inclusion of dephasing to change the picture.

In view of the success of our method for the dissipative XYZ model, we expect that it will yield new insights into a variety of dissipative spin systems, thanks to its ability to combine the inclusion of quantum effects at all length scales with the ability to study relatively large systems.

The assumption of the truncation of the correlation hierarchy to two-point correlations may be justified *a posteriori* by the effect of the environment, preventing quantum correlations from spreading significantly across the system, and from moving to progressively higher orders. Exceptions may exist to this picture, requiring the inclusion of higher-order correlations, such as the study of topological order in dissipative systems, which are known to relate to higher-order irreducible correlations [126] Extending the method to include k-point correlation functions leads to a computational cost scaling as $\mathcal{O}(N^k)$, which is still manageable, although the sizes that are practically accessible will be necessarily reduced.

The approach that we described is very flexible. In our present work we have focused on the steady state of the dissipative dynamics, but our approach also suggests the possibility of tracking the whole evolution of the system, starting from any initial state that is compatible with the truncation scheme of correlations. It does not rely on assumptions on lattice geometry such as locality, sparsity, or symmetries. Application to high-dimensional setups such as arbitrary graphs [127] would be straightforward. We further note that our method is compatible with a bosonic [9,36] or fermionic ansatz for the trajectory states, opening the way to the study of composite systems comprising different constituents. Finally, even in closed systems, the addition of fictitious dissipation has proven to be useful to obtain quantitatively meaningful results [128–130], and our method could be used in that context as well.

In the current stage of development of quantum technologies and the study of driven-dissipative physics accessible to experiments [18–21], there are a few important tasks: for example, assessing the impact of decoherence and dissipation in realistic quantum simulation and computing setups, and envisioning novel quantum states stabilized away from equilibrium by the competition between engineered unitary dynamics and the coupling to an engineered bath. We believe that the approach outlined in this work paves the way towards a systematic investigation of many-body phenomena in open quantum systems, and, as such, will contribute to the development of quantum technologies with open systems.

ACKNOWLEDGMENTS

Discussions with Raphaël Menu, Fabrizio Minganti, and Lennart Fernandes, as well as comments on the manuscript and support from Timothy C. H. Liew are gratefully acknowledged. This work is supported by UAntwerpen/DOCPRO/34878. W.V. gratefully acknowledges support from the Singapore Ministry of Education Tier 2 Grant No. MOET2EP50121-0020. D.H. and T.R. gratefully acknowledge the support of ANR ('EELS' project) and QuantERA ('MAQS' project). Part of the computational resources and services used in this work were provided by the VSC (Flemish Supercomputer Center), funded by the Research Foundation - Flanders (FWO) and the Flemish Government department EWI.

APPENDIX A: EVOLUTION EQUATIONS FOR THE $k = 2$ TRUNCATION SCHEME

In this section we detail the equations for the evolution of the single-spin and two-spin correlators stemming from the basis of the $k = 2$ truncation scheme. The equations for the single-spin expectation values read

$$d\langle\hat{\sigma}_s^x\rangle = \Big(-\frac{\gamma}{2}\langle\hat{\sigma}_s^x\rangle + 2J_y\sum_{s'}\langle\hat{\sigma}_{s'}^y\,\hat{\sigma}_s^z\rangle - 2J_z\sum_{s'}\langle\hat{\sigma}_{s'}^z\,\hat{\sigma}_s^y\rangle\Big)dt + \sqrt{\frac{\gamma}{2}}(1+\langle\hat{\sigma}_s^z\rangle - \langle\hat{\sigma}_s^x\rangle^2)dW_s^x + \sqrt{\frac{\gamma}{2}}\langle\hat{\sigma}_s^x\rangle\langle\hat{\sigma}_s^y\rangle dW_s^y$$
$$+\sqrt{\frac{\gamma}{2}}\sum_{j\neq s}\langle\hat{\delta}_s^x\hat{\delta}_j^x\rangle dW_j^x - \sqrt{\frac{\gamma}{2}}\sum_{j\neq s}\langle\hat{\delta}_s^x\hat{\delta}_j^y\rangle dW_j^y,$$
$$d\langle\hat{\sigma}_s^y\rangle = \Big(-\frac{\gamma}{2}\langle\hat{\sigma}_s^y\rangle + 2J_z\sum_{s'}\langle\hat{\sigma}_{s'}^z\,\hat{\sigma}_m^x\rangle - 2J_x\sum_{s'}\langle\hat{\sigma}_{s'}^x\,\hat{\sigma}_s^z\rangle\Big)dt - \sqrt{\frac{\gamma}{2}}\langle\hat{\sigma}_s^x\rangle\langle\hat{\sigma}_s^y\rangle dW_s^x - \sqrt{\frac{\gamma}{2}}(1+\langle\hat{\sigma}_s^z\rangle - \langle\hat{\sigma}_s^y\rangle^2)dW_s^y$$
$$+\sqrt{\frac{\gamma}{2}}\sum_{j\neq s}\langle\hat{\delta}_s^y\hat{\delta}_j^x\rangle dW_j^x - \sqrt{\frac{\gamma}{2}}\sum_{j\neq s}\langle\hat{\delta}_s^y\hat{\delta}_j^y\rangle dW_j^y,$$

$$d\langle\hat{\sigma}_s^z\rangle = \Big(-\gamma(\langle\hat{\sigma}_s^z\rangle + 1) + 2J_x \sum_{s'} \langle\hat{\sigma}_{s'}^x\, \hat{\sigma}_s^y\rangle - 2J_y \sum_{s'} \langle\hat{\sigma}_{s'}^y\, \hat{\sigma}_s^x\rangle \Big) dt - \sqrt{\frac{\gamma}{2}} \langle\hat{\sigma}_s^x\rangle (1 + \langle\hat{\sigma}_s^z\rangle) dW_s^x + \sqrt{\frac{\gamma}{2}} \langle\hat{\sigma}_s^y\rangle (1 + \langle\hat{\sigma}_s^z\rangle) dW_s^y$$
$$+ \sqrt{\frac{\gamma}{2}} \sum_{j \neq s} \langle\hat{\delta}_s^z \hat{\delta}_j^x\rangle dW_j^x - \sqrt{\frac{\gamma}{2}} \sum_{j \neq s} \langle\hat{\delta}_s^z \hat{\delta}_j^y\rangle dW_j^y,$$

where $\hat{\delta}_s^\alpha = \hat{\sigma}_s^\alpha - \langle\hat{\sigma}_s^\alpha\rangle$ and, consequently, $\langle\hat{\delta}_s^\alpha \hat{\delta}_m^\beta\rangle = \langle\hat{\sigma}_s^\alpha\, \hat{\sigma}_m^\beta\rangle - \langle\hat{\sigma}_s^\alpha\rangle\langle\hat{\sigma}_m^\beta\rangle$ indicates the two-site covariance.

Equation (8) leads to several contributions to the evolution of the covariances: two terms from the deterministic parts, an Ito term, and two noise terms from the stochastic part:

$$d\langle\hat{\delta}_s^\alpha \hat{\delta}_m^\beta\rangle = \langle(d_D\hat{\delta}_s^\alpha)\hat{\delta}_m^\beta\rangle + \langle\hat{\delta}_s^\alpha (d_D\hat{\delta}_m^\beta)\rangle + d_I\langle\hat{\delta}_s^\alpha \hat{\delta}_m^\beta\rangle + \langle(d_S\hat{\delta}_s^\alpha)\hat{\delta}_m^\beta\rangle + \langle\hat{\delta}_s^\alpha (d_S\hat{\delta}_m^\beta)\rangle. \tag{A1}$$

For the deterministic contributions, one can simply substitute

$$d_D\hat{\delta}_s^x = \Big(-\frac{\gamma}{2}\hat{\delta}_s^x + 2J_y \sum_{s'} \hat{\sigma}_s^z \hat{\sigma}_{s'}^y - 2J_z \sum_{s'} \hat{\sigma}_s^y \hat{\sigma}_{s'}^z \Big) dt, \tag{A2a}$$

$$d_D\hat{\delta}_s^y = \Big(-\frac{\gamma}{2}\hat{\delta}_s^y + 2J_z \sum_{s'} \hat{\sigma}_s^x \hat{\sigma}_{s'}^z - 2J_x \sum_{s'} \hat{\sigma}_s^z \hat{\sigma}_{s'}^x \Big) dt, \tag{A2b}$$

$$d_D\hat{\delta}_s^z = \Big(-\gamma\hat{\delta}_s^z + 2J_x \sum_{s'} \hat{\sigma}_s^y \hat{\sigma}_{s'}^x - 2J_y \sum_{s'} \hat{\sigma}_s^x \hat{\sigma}_{s'}^y \Big) dt. \tag{A2c}$$

For the stochastic terms, one has

$$\langle(d_S\hat{\delta}_s^x)\,\cdot\rangle = \sqrt{\frac{\gamma}{2}}(-2\langle\hat{\sigma}_s^x\rangle\langle\hat{\delta}_s^x\,\cdot\rangle + \langle\hat{\delta}_s^z\,\cdot\rangle) dW_s^x + \sqrt{\frac{\gamma}{2}}(\langle\hat{\sigma}_s^y\rangle\langle\hat{\delta}_s^x\,\cdot\rangle + \langle\hat{\sigma}_s^x\rangle\langle\hat{\delta}_s^y\,\cdot\rangle) dW_s^y, \tag{A3a}$$

$$\langle(d_S\hat{\delta}_s^y)\,\cdot\rangle = -\sqrt{\frac{\gamma}{2}}(\langle\hat{\sigma}_s^x\rangle\langle\hat{\delta}_s^y\cdot\rangle + \langle\hat{\sigma}_s^y\rangle\langle\hat{\delta}_s^x\,\cdot\rangle) dW_s^x + \sqrt{\frac{\gamma}{2}}(2\langle\hat{\sigma}_s^y\rangle\langle\hat{\delta}_s^y\cdot\rangle - \langle\hat{\delta}_s^z\cdot\rangle) dW_s^y, \tag{A3b}$$

$$\langle(d_S\hat{\delta}_s^z)\,\cdot\rangle = -\sqrt{\frac{\gamma}{2}}(\langle\hat{\delta}_s^x\cdot\rangle + \langle\hat{\sigma}_s^x\rangle\langle\hat{\delta}_s^z\cdot\rangle + \langle\hat{\sigma}_s^z\rangle\langle\hat{\delta}_s^x\cdot\rangle) dW_s^x + \sqrt{\frac{\gamma}{2}}(\langle\hat{\delta}_s^y\cdot\rangle + \langle\hat{\sigma}_s^y\rangle\langle\hat{\delta}_s^z\cdot\rangle + \langle\hat{\sigma}_s^z\rangle\langle\hat{\delta}_s^y\cdot\rangle) dW_s^y, \tag{A3c}$$

$$\langle\cdot\,(d_S\hat{\delta}_m^x)\rangle = \sqrt{\frac{\gamma}{2}}(-2\langle\hat{\sigma}_m^x\rangle\langle\cdot\hat{\delta}_m^x\rangle + \langle\cdot\hat{\delta}_m^z\rangle) dW_m^x + \sqrt{\frac{\gamma}{2}}(\langle\hat{\sigma}_m^y\rangle\langle\cdot\hat{\delta}_m^x\rangle + \langle\hat{\sigma}_m^x\rangle\langle\cdot\hat{\delta}_m^y\rangle) dW_m^y, \tag{A3d}$$

$$\langle\cdot\,(d_S\hat{\delta}_m^y)\rangle = -\sqrt{\frac{\gamma}{2}}(\langle\hat{\sigma}_m^x\rangle\langle\cdot\hat{\delta}_m^y\rangle + \langle\hat{\sigma}_m^y\rangle\langle\cdot\hat{\delta}_m^x\rangle) dW_m^x + \sqrt{\frac{\gamma}{2}}(2\langle\hat{\sigma}_m^y\rangle\langle\cdot\hat{\delta}_m^y\rangle - \langle\cdot\hat{\delta}_m^z\rangle) dW_m^y, \tag{A3e}$$

$$\langle\cdot\,(d_S\hat{\delta}_m^z)\rangle = -\sqrt{\frac{\gamma}{2}}(\langle\cdot\hat{\delta}_m^x\rangle + \langle\hat{\sigma}_m^x\rangle\langle\cdot\hat{\delta}_m^z\rangle + \langle\hat{\sigma}_m^z\rangle\langle\cdot\hat{\delta}_m^x\rangle) dW_m^x + \sqrt{\frac{\gamma}{2}}(\langle\cdot\hat{\delta}_m^y\rangle + \langle\hat{\sigma}_m^y\rangle\langle\cdot\hat{\delta}_m^z\rangle + \langle\hat{\sigma}_m^z\rangle\langle\cdot\hat{\delta}_m^y\rangle) dW_m^y, \tag{A3f}$$

where the center dots can be replaced with any operator $\hat{\delta}_m^\alpha$. Finally, the Ito terms give contributions such as

$$d_I\langle\hat{\delta}_s^x \hat{\delta}_m^x\rangle = -\frac{\gamma}{2}[(1 + \langle\hat{\sigma}_s^z\rangle - \langle\hat{\sigma}_s^x\rangle^2)\langle\hat{\delta}_m^x \hat{\delta}_s^x\rangle + \langle\hat{\sigma}_s^x\rangle\langle\hat{\sigma}_s^y\rangle\langle\hat{\delta}_m^x \hat{\delta}_s^y\rangle + (s \leftrightarrow m)]dt - \frac{\gamma}{2} \sum_{j \neq s,m} [\langle\hat{\delta}_s^x \hat{\delta}_j^x\rangle\langle\hat{\delta}_j^x \hat{\delta}_m^x\rangle + \langle\hat{\delta}_s^x \hat{\delta}_j^y\rangle\langle\hat{\delta}_j^y \hat{\delta}_m^x\rangle]dt. \tag{A4}$$

Equations (A2) contain the three-spin terms of the form $\langle\hat{\sigma}_s^\alpha \hat{\sigma}_{s'}^\beta \hat{\delta}_m^\gamma\rangle$. We can reduce them to functions of single- and two-spin terms by assuming the vanishing of the third-order cumulant; in doing so, we distinguish between the cases when the s' index is and is not equal to m. If $s' = m$, $\hat{\sigma}_m^\beta \hat{\sigma}_m^\gamma = \hat{\sigma}_m^{\beta\gamma}$ is another single spin operator and

$$\langle\hat{\sigma}_s^\alpha \hat{\sigma}_m^\beta \hat{\delta}_m^\gamma\rangle = \langle\hat{\delta}_s^\alpha \hat{\delta}_m^{\beta\gamma}\rangle + \langle\hat{\sigma}_s^\alpha\rangle\langle\hat{\sigma}_m^{\beta\gamma}\rangle - \langle\hat{\sigma}_m^\gamma\rangle\langle\hat{\sigma}_s^\alpha\, \hat{\sigma}_m^\beta\rangle; \tag{A5}$$

otherwise,

$$\langle\hat{\sigma}_s^\alpha\hat{\sigma}_{s'}^\beta\hat{\delta}_m^\gamma\rangle = \langle\hat{\sigma}_s^\alpha\rangle\langle\hat{\delta}_{s'}^\beta\hat{\delta}_m^\gamma\rangle + \langle\hat{\sigma}_{s'}^\beta\rangle\langle\hat{\delta}_s^\alpha\hat{\delta}_m^\gamma\rangle. \tag{A6}$$

Similarly,

$$\langle\hat{\delta}_s^\alpha\hat{\sigma}_s^\beta\hat{\sigma}_m^\gamma\rangle = \langle\hat{\delta}_s^{\alpha\beta}\hat{\delta}_m^\gamma\rangle + \langle\hat{\sigma}_s^{\alpha\beta}\rangle\langle\hat{\sigma}_m^\gamma\rangle - \langle\hat{\sigma}_s^\alpha\rangle\langle\hat{\sigma}_s^\beta\,\hat{\sigma}_m^\gamma\rangle, \tag{A7}$$

and, for $s \neq m'$,

$$\langle\hat{\delta}_s^\alpha\hat{\sigma}_{m'}^\beta\hat{\sigma}_m^\gamma\rangle = \langle\hat{\sigma}_{m'}^\beta\rangle\langle\hat{\delta}_s^\alpha\hat{\delta}_m^\gamma\rangle + \langle\hat{\sigma}_m^\gamma\rangle\langle\hat{\delta}_s^\alpha\hat{\delta}_m^\beta\rangle. \tag{A8}$$

APPENDIX B: FINITE MEASUREMENT EFFICIENCIES

We find that the numerical simulation of the quantum trajectory $k = 2$ equations are subject to numerical instabilities in various parameter regimes. More specifically, the expectation values tend to diverge at very short time scales, leading to unphysical results and ultimately numerical "not a number" (NaN) results. These numerical instabilities are caused by the noise terms coupled to the second-order cumulants [Eqs. (A3)], or second-order noise terms in short, and are very hard to control or suppress. However, not including the second-order noise terms allows one to simulate the equations and yield physical results with little to no numerical instabilities. We now show, through a numerical example, that these second-order noise terms are not important, and can be neglected from the equations, by using the concept of measuring efficiency. This method will allow us to profit from the numerical stability of the standard master equation approach, in combination with the increase in the method's complexity due to the trajectory approach. We first recall the concept and then apply it to the *XYZ* model studied in the main text, the results of which are shown in Fig. 11 below.

In the quantum trajectory formalism one assumes the existence of perfect detectors continuously monitoring the system of interest. This leads to Eq. (7). However, one can equivalently derive equations for the more general case where the detector has a finite efficiency $0 \leq \eta \leq 1$ [71].

Indeed, one can rewrite Eq. (2) as

$$\begin{aligned}\partial_t\hat{\rho} = &-i[\hat{\mathrm{H}}\hat{\rho}] + \frac{1}{2}\sum_j(1-\eta)(2\hat{\Gamma}_j\hat{\rho}\hat{\Gamma}_j^\dagger - \hat{\Gamma}_j^\dagger\hat{\Gamma}_j\hat{\rho} - \hat{\rho}\hat{\Gamma}_j^\dagger\hat{\Gamma}_j) \\ &+ \frac{1}{2}\sum_j\eta(2\hat{\Gamma}_j\hat{\rho}\hat{\Gamma}_j^\dagger - \hat{\Gamma}_j^\dagger\hat{\Gamma}_j\hat{\rho} - \hat{\rho}\hat{\Gamma}_j^\dagger\hat{\Gamma}_j),\end{aligned} \tag{B1}$$

where we have rewritten the original dissipator as two individual dissipators with Lindblad operators $\sqrt{1-\eta}\hat{\Gamma}_j$ and $\sqrt{\eta}\hat{\Gamma}_j$. We can imagine now that only the part proportional to η contributes to the noise term in the stochastic Schrödinger's equation emerging in the quantum state diffusion approach, Eq. (7). Physically, this process corresponds to a situation in which the information (i.e., photon current) leaking out of the system is collected with a finite efficiency $\eta \leq 1$. One can then straightforwardly show that this yields the following equation for the expectation value of an operator $\hat{O}$:

$$\begin{aligned}d\langle\hat{\mathrm{O}}\rangle = &\, i\langle[\hat{\mathrm{H}}\hat{\mathrm{O}}]\rangle dt - \frac{1}{2}\sum_j(\langle\hat{\Gamma}_j^\dagger[\hat{\Gamma}_j\hat{\mathrm{O}}]\rangle - \langle[\hat{\Gamma}_j^\dagger\hat{\mathrm{O}}]\hat{\Gamma}_j\rangle)dt \\ &+ \sqrt{\eta}\sum_j(\langle\hat{\Gamma}_j^\dagger(\hat{O} - \langle\hat{O}\rangle)\rangle dZ_j \\ &+ \langle(\hat{O} - \langle\hat{O}\rangle)\hat{\Gamma}_j\rangle dZ_j^*).\end{aligned} \tag{B2}$$

Including a finite efficiency for the continuous monitoring process thus leads to only a factor $\sqrt{\eta}$ in the noise part of the trajectory formalism. A measuring efficiency $\eta = 1$ brings us back to the original quantum trajectory equations, while for $\eta = 0$, one retrieves the master equation approach to correlation hierarchies [Eq. (3)]. For the latter, no noise terms are present (on any cumulant) and the earlier mentioned numerical instabilities are absent In practice, the imperfect measuring efficiency η makes the simulation of the equations numerically more stable. As a result, it allows one to numerically solve the equations using the $k = 2$ quantum trajectory formalism until the numerical instability becomes unmanageable. Note that such a formalism is physical by itself [71], and naturally compatible with our approach.

Hence, we use this finite measuring efficiency formalism to solve the $k = 2$ quantum trajectory equations for various values of η and show that their results are identical to the $k = 2$ quantum trajectories *without* second-order noise terms (and of course with the same respective η, i.e., noise coefficients to the first-order cumulants). Such an analysis allows us to extrapolate the validity of the $k = 2$ quantum trajectory approach without second-order noise terms at full measuring efficiency ($\eta = 1$), and thus in the regime where one profits most of the trajectory approach with respect to the master equation approach ($\eta = 0$).

We now revisit the results for the dissipative *XYZ* model, by focusing on the steady-state structure factor $S_{\mathrm{SS}}^{\phi\phi}(0)$ for the ϕ spin components displaying the strongest correlations (see Sec. IV A). In Figs. 11(a) and 11(b) we show the $k = 2$ quantum trajectory results with and without second-order noise contributions [Eqs. (A3)] for various values of η of a 7×7 lattice. We generally observe very good agreement between the results excluding the second-noise terms and those including them (when available) for various values of η, showing that those noise contributions are in fact negligible whenever they do not lead to numerical instabilities.

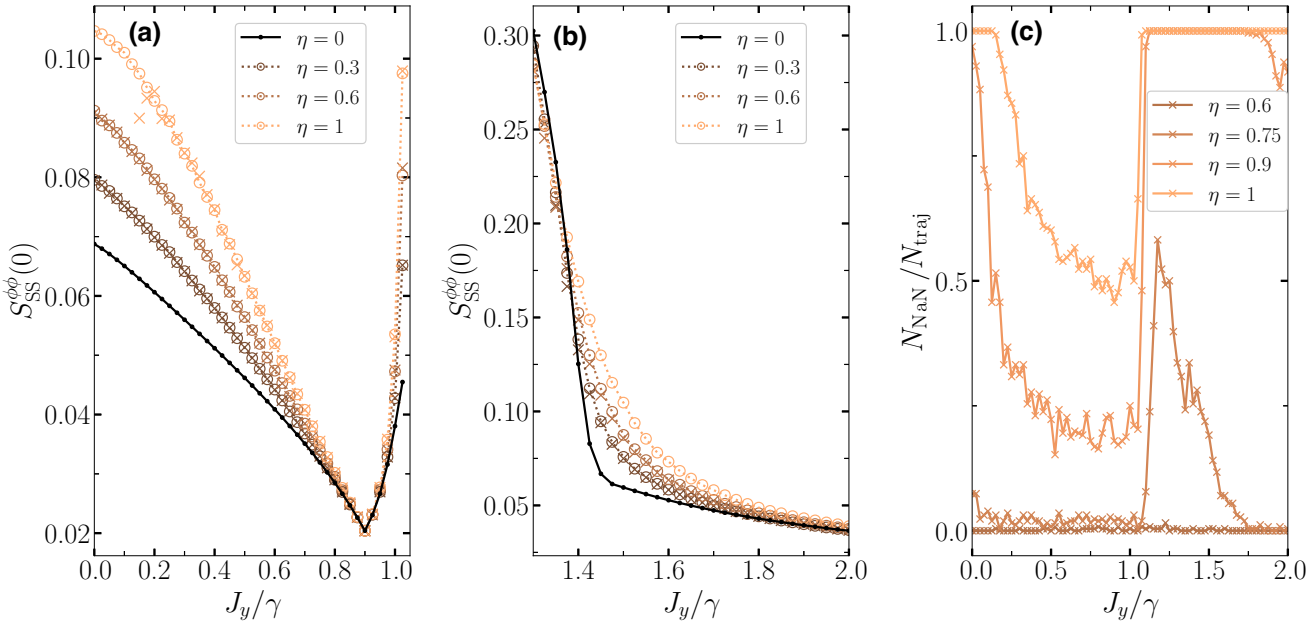

FIG. 11. (a),(b) Steady-state structure factor $S^{\phi\phi}_{\mathrm{SS}}(0)$ on a 7×7 lattice for various measuring efficiencies η, with second-order noise contributions (crosses) and without second-order noise contributions (dotted lines with circles), for two regions of the phase diagram. (c) Number of diverging, i.e., NaN, trajectories N_{NaN} with respect to the total number of trajectories N_{traj}. Only results with second-order noise terms (solid lines with crosses) are shown as results without second-order noise terms are all located at (approximately) zero. The number of trajectories for the results in all panels is $N_{\mathrm{traj}} = 256$, and time averages are taken over the time interval $t\gamma \in [75; 150]$.

Note that, for higher values of η, occasional results deviate for values of $J_y/\gamma \approx 0.1$ [see Fig. 11(a)], which is due to the increasing number of diverging trajectories. We denote this number N_{NaN} and show this rate with respect to the total number of trajectories N_{traj} in Fig. 11(c). Every time a trajectory diverges, we discard the entire trajectory and do not use it to gather statistics on the system. We note that such omission of divergent trajectories is mathematically justified under quite general conditions [131]. Because of the very low number of nondiverging trajectories at high measuring efficiencies, the gathered statistics will evidently be low. Hence, some deviations from the (stable) results where the second-order noise term has been omitted appear in the finite numerics. For example, for the highest values of η, the number of diverging trajectories is equal to the number of simulated trajectories for the highest (and lowest) values of J_y/γ shown in Fig. 11(c). This in turn results in a lack of results for the $k = 2$ quantum trajectory approach with noise terms, i.e., the original problem.

Nevertheless, as the efficiency η is increased, across the parameter regime, one still observes the correspondence between the results with and without noise terms. Extrapolating these results in the limit of $\eta \to 1$ (i.e., assuming that the second-order noise terms remain negligible at efficiency $\eta = 1$ over the entire range of parameters that we explore—including in parameter regions for which all trajectories become numerically unstable when second-order noise terms are included), we can conclude that the omission of the second-order noise terms is legitimate. All the results presented in the main text for the $k = 2$ truncation scheme are therefore solutions to equations with $\eta = 1$ with the omission of second-order noise terms.

APPENDIX C: SECOND AND FOURTH MOMENTS OF THE *xy* SPIN COMPONENTS

We show results for the (steady-state) second and fourth moments of $(1/N)\sum_j \hat{\sigma}^x_j$ and $(1/N)\sum_j \hat{\sigma}^y_j$ in Figs. 12(a)–12(d). Note that the second moment is identical to the structure factor from Eq. (25), $S^{\alpha\alpha}_{\mathrm{SS}}(\mathbf{k} = 0) = m^{\alpha}_2$. The remarkable correspondence with the exact results shown in Fig. 12(a) is thus identical to that discussed in Fig. 1(a). Nonetheless, panels (b)–(d) of Fig. 12 show that this correspondence to the exact results is not limited to the second moment, but also persists in the fourth moment for both the $\hat{\sigma}^x$ and $\hat{\sigma}^y$ spin components. Moreover, the correspondence of the second moment m^y_2 and the fourth moment m^y_4 is even more convincing than that for m^x_2 and m^x_4.

The agreement of the fourth moment of the spin components with exact diagonalization shows that the truncation scheme of the cumulant hierarchy to second order does *not* lead to a significant loss in accuracy when looking at higher-order correlators. This observation vindicates the working assumption underlying our approach, namely,

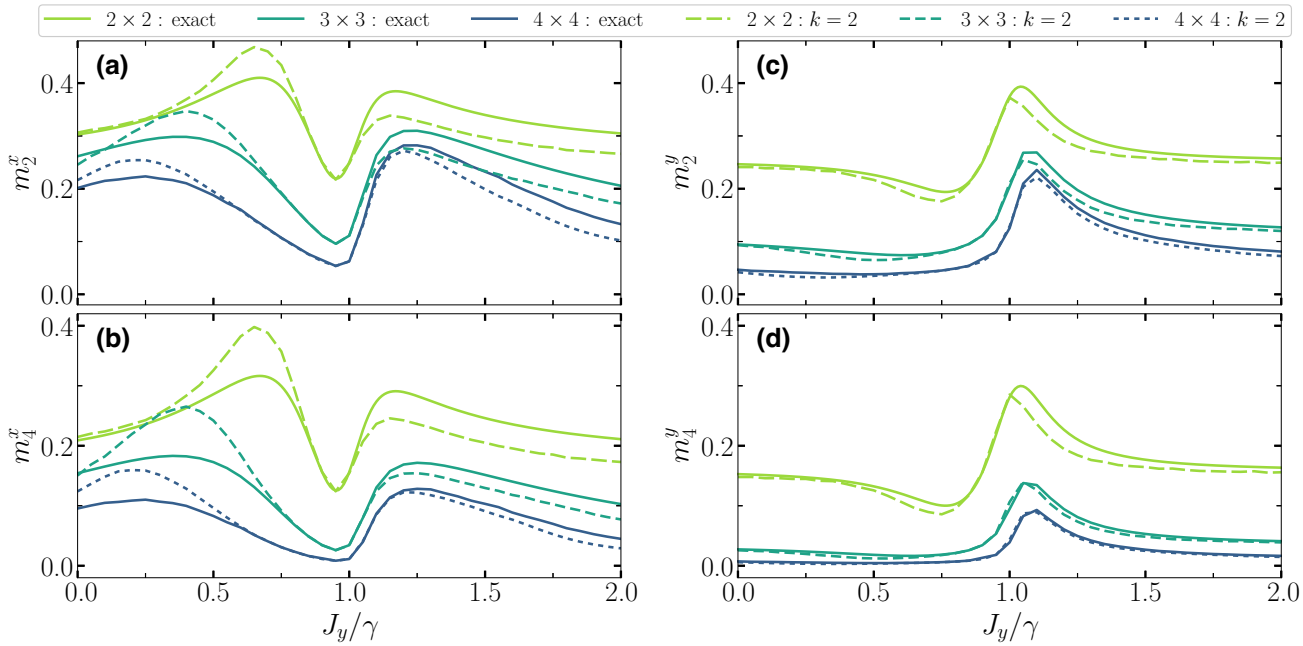

FIG. 12. Second (a,c) and fourth (b,d) moments for the $\hat{\sigma}^x$ (a,b) and $\hat{\sigma}^y$ (c,d) spin components obtained with the $k = 2$ truncation scheme (dashed lines), compared with the exact solution (solid lines) for three different system sizes. The exact results correspond to a direct solution of the master equation for $N < 4$, and to its stochastic unraveling for $N = 4$. The $k = 2$ results are obtained using $N_{\text{traj}} \approx 250$ trajectories, and time averaging is performed over the time interval $t\gamma \in [75; 150]$.

the fact that cumulants of order higher than $k = 2$ are essentially negligible in the steady state.

APPENDIX D: FINITE-SIZE SCALING OF THE $k = 1$ RESULTS

In the main text, using the $k = 2$ cumulant truncation scheme, we have shown that the phase transitions belong to the universality class of the classical 2D Ising model, and hence the critical fluctuations are of a classical nature. It may thus be tempting to think that the $k = 1$ (Gutzwiller) trajectories are already sufficient to describe this behavior, as they are expected to capture classical fluctuations without any *a priori* assumption or limitation on their spatial structure.

However, as we can see in Fig. 13 for the paramagnetic-to-ferromagnetic transition (at $J_x/\gamma = 0.9$, $J_y/\gamma \approx 1$) the $k = 1$ results are incompatible with the 2D Ising universality class.

Figures 13(a) and 13(b) show the rescaled structure factor $S_{\text{SS}}^{\phi\phi}(0)L^{2\beta/\nu}$ using 2D classical Ising exponents, which do not lead to a clear collapse of the curves for different system sizes, even in the vicinity of the putative critical point. In fact, different combinations of critical exponents can give a better collapse. In particular, a decent collapse is obtained when one takes $\beta = \nu = 1/2$, i.e., the mean-field critical exponents, as shown in Figs. 13(c) and 13(d).

For the second transition (from ferromagnetism back to paramagnetism) at even higher J_y values, it was already clear from earlier works that the Gutzwiller trajectory approach [41] and its cluster extensions [44] predict a size-dependent sudden drop in the structure factor instead of a set of smooth curves that find a common crossing upon rescaling, which would be the expected behavior at a continuous phase transition.

APPENDIX E: SCALING OF THE TRANSVERSE MAGNETIZATION DERIVATIVE AT THE 2D ISING TRANSITION

In this section we discuss the expected scaling of the derivative of the transverse magnetization with respect to the control parameter of the transition at the thermal phase transition of the 2D Ising model. This discussion serves as a basis for the scaling analysis proposed in Sec. IV D for this quantity at the dissipative transition of the 2D *XYZ* model.

For the sake of definiteness, we use as a reference model the transverse field Ising model, with Hamiltonian

$$\hat{H} = -J \sum_{\langle ij \rangle} \hat{\sigma}_i^x \hat{\sigma}_j^x - \Gamma \sum_i \hat{\sigma}_i^z \tag{E1}$$

defined on the same square lattice as the *XYZ* model investigated in the main text. Although the above model has a well-known quantum phase transition in the ground state, we focus only on its thermal properties, and in particular on the fact that it has a line of thermal 2D Ising transitions

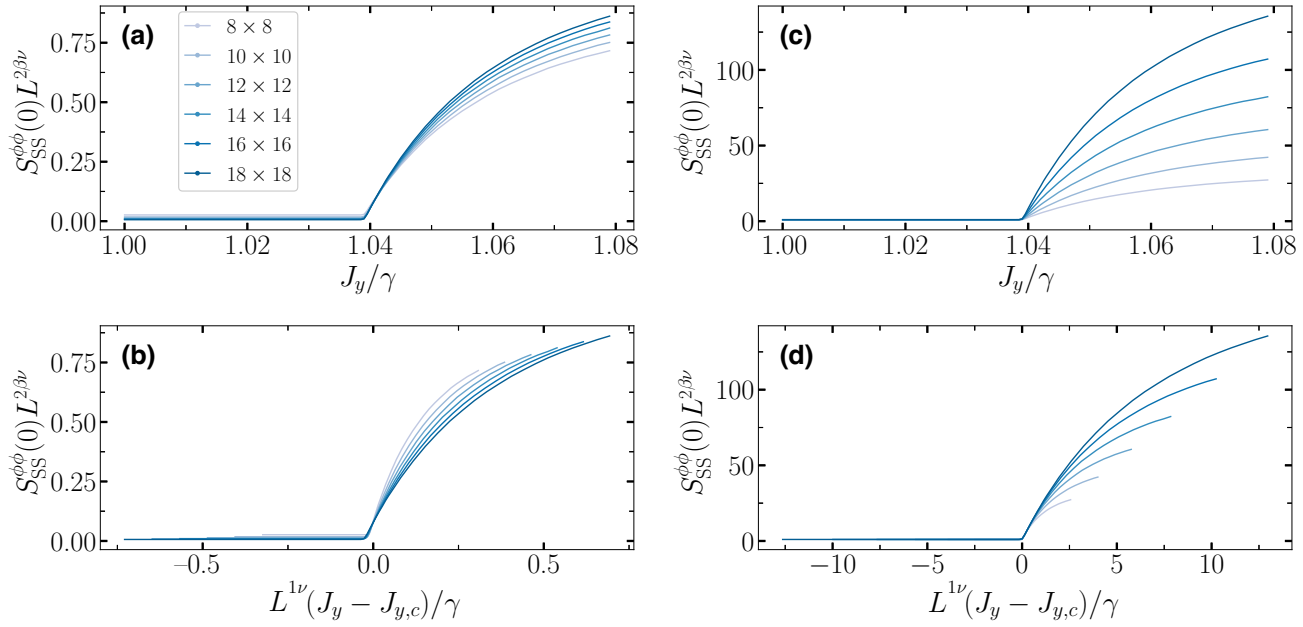

FIG. 13. Finite-size scaling analysis of the $k = 1$ results for the structure factor $S^{\phi\phi}_{\rm SS}(0)$: (a) rescaled structure factor $S^{\phi\phi}_{\rm SS}(0)L^{2\beta/\nu}$ using 2D Ising exponents ($\nu = 1$ and $\beta = 1/8$); (b) full scaling plot with the same exponents, using the critical point $J_{y,c} = 1.0405$; (c) rescaled structure factor $S^{\phi\phi}_{\rm SS}(0)L^{2\beta/\nu}$ using mean-field exponents ($\nu = 1/2$ and $\beta = 1/2$); (d) full scaling plot with the same exponents, using $J_{y,c} = 1.039$. All results stem from $N_{\rm traj} \approx 32$ trajectories, and they are time averaged over the time interval $t\gamma \in [700; 1000]$.

at temperatures $T_c(\Gamma)$ that decrease with increasing Γ, and eventually vanish at the quantum critical point.

In the vicinity of the critical line, the singular part of the free-energy density is expected to scale as

$$f_s(T, \Gamma) \sim |T - T_c(\Gamma)|^{2-\alpha}, \tag{E2}$$

which implies that the transverse magnetization $m^z = \langle \sigma^z_i \rangle$ has singular part

$$m^z = -\frac{\partial f_s}{\partial \Gamma} \sim (2-\alpha)\frac{dT_c}{d\Gamma}|T - T_c(\Gamma)|^{1-\alpha}, \tag{E3}$$

while the derivative of this magnetization with respect to the control parameter of the transition (namely, the temperature T) exhibits a singularity of the form

$$\frac{\partial m^z}{\partial T} = -\frac{\partial^2 f_s}{\partial \Gamma \partial T} \sim (2-\alpha)(1-\alpha)\frac{dT_c}{d\Gamma}|T - T_c(\Gamma)|^{-\alpha}, \tag{E4}$$

namely, it is has the same singular behavior as the specific heat

$$c_v = -T\frac{\partial^2 f_s}{\partial T^2} \sim (2-\alpha)(1-\alpha)|T - T_c(\Gamma)|^{-\alpha}. \tag{E5}$$

The 2D Ising universality class has $\alpha = 0$, meaning that the scaling dimension of the specific heat, α/ν, is also vanishing. Yet this result still leaves room for a specific heat diverging at the transition as $\log L$, where L is the linear size of the lattice. Hence we expect that this same scaling property is also shared with the temperature derivative of the transverse magnetization $\partial m^z/\partial T$. We have verified that this is indeed the case on quantum Monte Carlo data for the thermal transition of the 2D Ising model in a transverse field. We can therefore expect the same scaling behavior to be shared with $\gamma(dm^z/dJ_y)$ at the dissipative transition of the 2D *XYZ* model if this transition is to comply with the 2D Ising universality class; the logarithmic divergence of $\partial m^z/\partial T$ is clearly exhibited in Sec. IV D.

[1] A. G. J. MacFarlane, J. P. Dowling, and G. J. Milburn, Quantum technology: The second quantum revolution, Philos. Trans. R. Soc. London Ser. A: Math., Phys. Eng. Sci. **361**, 1655 (2003).

[2] J. Preskill, Quantum computing and the entanglement frontier, (2012), ArXiv:1203.5813.

[3] A. Acín, I. Bloch, H. Buhrman, T. Calarco, C. Eichler, J. Eisert, D. Esteve, N. Gisin, S. J. Glaser, F. Jelezko, S. Kuhr, M. Lewenstein, M. F. Riedel, P. O. Schmidt, R. Thew, A. Wallraff, I. Walmsley, and F. K. Wilhelm, The quantum technologies roadmap: A European community view, New J. Phys. **20**, 080201 (2018).

[4] E. Altman, *et al.*, Quantum Simulators: Architectures and Opportunities, PRX Quantum **2**, 017003 (2021).

[5] M. B. Plenio, S. F. Huelga, A. Beige, and P. L. Knight, Cavity-loss-induced generation of entangled atoms, Phys. Rev. A **59**, 2468 (1999).

[6] F. Verstraete, M. M. Wolf, and J. I. Cirac, Quantum computation and quantum-state engineering driven by dissipation, Nat. Phys. **5**, 633 (2009).

[7] F. Minganti, A. Biella, N. Bartolo, and C. Ciuti, Spectral theory of Liouvillians for dissipative phase transitions, Phys. Rev. A **98**, 042118 (2018).

[8] L. M. Sieberer, M. Buchhold, and S. Diehl, Keldysh field theory for driven open quantum systems, Rep. Prog. Phys. **79**, 096001 (2016).

[9] W. Verstraelen, R. Rota, V. Savona, and M. Wouters, Gaussian trajectory approach to dissipative phase transitions: The case of quadratically driven photonic lattices, Phys. Rev. Res. **2**, 022037 (2020).

[10] D. O. Krimer and M. Pletyukhov, Few-Mode Geometric Description of a Driven-Dissipative Phase Transition in an Open Quantum System, Phys. Rev. Lett. **123**, 110604 (2019).

[11] T. Tomita, S. Nakajima, I. Danshita, Y. Takasu, and Y. Takahashi, Observation of the Mott insulator to superfluid crossover of a driven-dissipative Bose-Hubbard system, Sci. Adv. **3**, 1701513 (2017).

[12] S. Diehl, A. Micheli, A. Kantian, B. Kraus, H. P. Büchler, and P. Zoller, Quantum states and phases in driven open quantum systems with cold atoms, Nat. Phys. **4**, 878 (2008).

[13] T. Fink, A. Schade, S. Höfling, C. Schneider, and A. Imamoglu, Signatures of a dissipative phase transition in photon correlation measurements, Nat. Phys. **14**, 365 (2018).

[14] M. Fitzpatrick, N. M. Sundaresan, A. C. Y. Li, J. Koch, and A. A. Houck, Observation of a Dissipative Phase Transition in a One-Dimensional Circuit QED Lattice, Phys. Rev. X **7**, 011016 (2017).

[15] A. D. Greentree, C. Tahan, J. H. Cole, and L. C. L. Hollenberg, Quantum phase transitions of light, Nat. Phys. **2**, 856 (2006).

[16] P. Kirton, M. M. Roses, J. Keeling, and E. G. Dalla Torre, Introduction to the Dicke model: from equilibrium to nonequilibrium, and vice versa, Adv. Quantum Technol. **2**, 1800043 (2019).

[17] H. J. Carmichael, Breakdown of Photon Blockade: A Dissipative Quantum Phase Transition in Zero Dimensions, Phys. Rev. X **5**, 031028 (2015).

[18] I. Carusotto, A. A. Houck, A. J. Kollár, P. Roushan, D. I. Schuster, and J. Simon, Photonic materials in circuit quantum electrodynamics, Nat. Phys. **16**, 268 (2020).

[19] D. E. Chang, V. Vuletić, and M. D. Lukin, Quantum nonlinear opticsâ–photon by photon, Nat. Photon. **8**, 685 (2014).

[20] D. Leibfried, R. Blatt, C. Monroe, and D. Wineland, Quantum dynamics of single trapped ions, Rev. Mod. Phys. **75**, 281 (2003).

[21] A. Kavokin, J. J. Baumberg, G. Malpuech, and F. P. Laussy, *Microcavities* (Oxford University Press, Oxford, 2007).

[22] M. Hartmann, F. Brandão, and M. Plenio, Quantum many-body phenomena in coupled cavity arrays, Laser Photon. Rev. **2**, 527 (2008).

[23] T. E. Lee, S. Gopalakrishnan, and M. D. Lukin, Unconventional Magnetism via Optical Pumping of Interacting Spin Systems, Phys. Rev. Lett. **110**, 257204 (2013).

[24] N. Mohseni, P. L. McMahon, and T. Byrnes, Ising machines as hardware solvers of combinatorial optimization problems, Nature Reviews Physics (2022).

[25] D. Monroe, Neuromorphic computing gets ready for the (really) big time, Commun. ACM **57**, 13 (2014).

[26] D. Ballarini, A. Gianfrate, R. Panico, A. Opala, S. Ghosh, L. Dominici, V. Ardizzone, M. De Giorgi, G. Lerario, G. Gigli, T. C. H. Liew, M. Matuszewski, and D. Sanvitto, Polaritonic neuromorphic computing outperforms linear classifiers, Nano Lett. **20**, 3506 (2020).

[27] R. A. Bravo, K. Najafi, X. Gao, and S. F. Yelin, Quantum Reservoir Computing Using Arrays of Rydberg Atoms, PRX Quantum **3**, 030325 (2022).

[28] M. Napolitano, M. Koschorreck, B. Dubost, N. Behbood, R. J. Sewell, and M. W. Mitchell, Interaction-based quantum metrology showing scaling beyond the Heisenberg limit, Nature **471**, 486 (2011).

[29] A. J. Daley, Quantum trajectories and open many-body quantum systems, Adv. Phys. **63**, 77 (2014).

[30] H. Weimer, A. Kshetrimayum, and R. Orús, Simulation methods for open quantum many-body systems, Rev. Mod. Phys. **93**, 015008 (2021).

[31] P. Deuar, A. Ferrier, M. Matuszewski, G. Orso, and M. H. Szymanska, Fully Quantum Scalable Description of Driven-Dissipative Lattice Models, PRX Quantum **2**, 010319 (2021).

[32] S. Finazzi, A. Le Boité, F. Storme, A. Baksic, and C. Ciuti, Corner-Space Renormalization Method for Driven-Dissipative Two-Dimensional Correlated Systems, Phys. Rev. Lett. **115**, 080604 (2015).

[33] D. Huybrechts and M. Wouters, Dynamical hysteresis properties of the driven-dissipative Bose-Hubbard model with a Gutzwiller Monte Carlo approach, Phys. Rev. A **102**, 053706 (2020).

[34] N. Ramusat and V. Savona, A quantum algorithm for the direct estimation of the steady state of open quantum systems, Quantum **5**, 399 (2021).

[35] W. Verstraelen, *Gaussian quantum trajectories for the variational simulation of open quantum systems, with photonic applications*, Ph.D. thesis, University of Antwerp (2020), https://hdl.handle.net/10067/1699290151162165141.

[36] W. Verstraelen and M. Wouters, Gaussian quantum trajectories for the variational simulation of open quantum-optical systems, Appl. Sci. **8**, 1427 (2018).

[37] C. D. Mink, D. Petrosyan, and M. Fleischhauer, Hybrid discrete-continuous truncated Wigner approximation for driven, dissipative spin systems, (2022), arXiv preprint ArXiv:2203.17120.

[38] I. H. Deutsch, Harnessing the Power of the Second Quantum Revolution, PRX Quantum **1**, 020101 (2020).

[39] J. Jin, A. Biella, O. Viyuela, L. Mazza, J. Keeling, R. Fazio, and D. Rossini, Cluster Mean-Field Approach to the Steady-State Phase Diagram of Dissipative Spin Systems, Phys. Rev. X **6**, 031011 (2016).

[40] R. Rota, F. Storme, N. Bartolo, R. Fazio, and C. Ciuti, Critical behavior of dissipative two-dimensional spin lattices, Phys. Rev. B **95**, 134431 (2017).

[41] W. Casteels, R. M. Wilson, and M. Wouters, Gutzwiller Monte Carlo approach for a critical dissipative spin model, Phys. Rev. A **97**, 062107 (2018).

[42] R. Rota, F. Minganti, A. Biella, and C. Ciuti, Dynamical properties of dissipative XYZ Heisenberg lattices, New J. Phys. **20**, 045003 (2018).

[43] A. Biella, J. Jin, O. Viyuela, C. Ciuti, R. Fazio, and D. Rossini, Linked cluster expansions for open quantum systems on a lattice, Phys. Rev. B **97**, 035103 (2018).

[44] D. Huybrechts and M. Wouters, Cluster methods for the description of a driven-dissipative spin model, Phys. Rev. A **99**, 043841 (2019).

[45] A. Nagy and V. Savona, Variational Quantum Monte Carlo Method with a Neural-Network Ansatz for Open Quantum Systems, Phys. Rev. Lett. **122**, 250501 (2019).

[46] D. Huybrechts, F. Minganti, F. Nori, M. Wouters, and N. Shammah, Validity of mean-field theory in a dissipative critical system: Liouvillian gap, $\mathbb{PT}$-symmetric antigap, and permutational symmetry in the *XYZ* model, Phys. Rev. B **101**, 214302 (2020).

[47] X. Li and J. Jin, Nonuniform phases in the geometrically frustrated dissipative XYZ model, Phys. Rev. B **103**, 035127 (2021).

[48] D. Kilda, A. Biella, M. Schiro, R. Fazio, and J. Keeling, On the stability of the infinite projected entangled pair operator ansatz for driven-dissipative 2D lattices, SciPost Phys. Core **4**, 005 (2021).

[49] C. Mc Keever and M. H. Szymańska, Stable iPEPO Tensor-Network Algorithm for Dynamics of Two-Dimensional Open Quantum Lattice Models, Phys. Rev. X **11**, 021035 (2021).

[50] E. T. Owen, J. Jin, D. Rossini, R. Fazio, and M. J. Hartmann, Quantum correlations and limit cycles in the driven-dissipative Heisenberg lattice, New J. Phys. **20**, 045004 (2018).

[51] C. Chan, T. E. Lee, and S. Gopalakrishnan, Limit-cycle phase in driven-dissipative spin systems, Phys. Rev. A **91**, 051601 (2015).

[52] X. Li, Y. Li, and J. Jin, Steady-state phases of the dissipative spin-1/2 XYZ model with frustrated interactions, Phys. Rev. B **104**, 155130 (2021).

[53] X. Li, Y. Li, and J. Jin, Steady-state susceptibility in continuous phase transitions of dissipative systems, Phys. Rev. A **105**, 052226 (2022).

[54] G. Tóth and D. Petz, Extremal properties of the variance and the quantum Fisher information, Phys. Rev. A **87**, 032324 (2013).

[55] G. Lindblad, On the generators of quantum dynamical semigroups, Commun. Math. Phys. **48**, 119 (1976).

[56] V. Gorini, A. Kossakowski, and E. C. G. Sudarshan, Completely positive dynamical semigroups of n-level systems, J. Math. Phys. **17**, 821 (1976).

[57] H. Breuer and F. Petruccione, *The Theory of Open Quantum Systems* (OUP Oxford, Oxford, 2007).

[58] D. Tupkary, A. Dhar, M. Kulkarni, and A. Purkayastha, Fundamental limitations in Lindblad descriptions of systems weakly coupled to baths, Phys. Rev. A **105**, 032208 (2022).

[59] M. Cattaneo, G. De Chiara, S. Maniscalco, R. Zambrini, and G. L. Giorgi, Collision Models Can Efficiently Simulate any Multipartite Markovian Quantum Dynamics, Phys. Rev. Lett. **126**, 130403 (2021).

[60] F. Barra, The thermodynamic cost of driving quantum systems by their boundaries, Sci. Rep. **5**, 14873 (2015).

[61] J. Jin, W.-B. He, F. Iemini, D. Ferreira, Y.-D. Wang, S. Chesi, and R. Fazio, Determination of the critical exponents in dissipative phase transitions: Coherent anomaly approach, Phys. Rev. B **104**, 214301 (2021).

[62] M. J. Hartmann and G. Carleo, Neural-Network Approach to Dissipative Quantum Many-Body Dynamics, Phys. Rev. Lett. **122**, 250502 (2019).

[63] F. Vicentini, A. Biella, N. Regnault, and C. Ciuti, Variational Neural-Network Ansatz for Steady States in Open Quantum Systems, Phys. Rev. Lett. **122**, 250503 (2019).

[64] N. Yoshioka and R. Hamazaki, Constructing neural stationary states for open quantum many-body systems, Phys. Rev. B **99**, 214306 (2019).

[65] A. Kshetrimayum, H. Weimer, and R. Orús, A simple tensor network algorithm for two-dimensional steady states, Nat. Commun. **8**, 1291 (2017).

[66] V. P. Singh and H. Weimer, Driven-Dissipative Criticality within the Discrete Truncated Wigner Approximation, Phys. Rev. Lett. **128**, 200602 (2022).

[67] J. Huber, A. M. Rey, and P. Rabl, Realistic simulations of spin squeezing and cooperative coupling effects in large ensembles of interacting two-level systems, Phys. Rev. A **105**, 013716 (2022).

[68] M. Van Regemortel, W. Casteels, I. Carusotto, and M. Wouters, Spontaneous Beliaev-Landau scattering out of equilibrium, Phys. Rev. A **96**, 053854 (2017).

[69] C. Gardiner and P. Zoller, *Quantum Noise: A Handbook of Markovian and Non-Markovian Quantum Stochastic Methods with Applications to Quantum Optics* (Springer, Berlin, 2004).

[70] H. Carmichael, *Statistical Methods in Quantum Optics 2: Non-Classical Fields* (Springer Berlin Heidelberg, Berlin, 2007).

[71] H. Wiseman and G. Milburn, *Quantum Measurement and Control* (Cambridge University Press, Cambridge, 2010).

[72] T. A. Brun, A simple model of quantum trajectories, Am. J. Phys. **70**, 719 (2002).

[73] H. Carmichael, *An Open Systems Approach to Quantum Optics Lectures Presented at the Université Libre de Bruxelles, October 28 to November 4, 1991* (Springer, Brussels, 1993).

[74] J. Dalibard, Y. Castin, and K. Mølmer, Wave-Function Approach to Dissipative Processes in Quantum Optics, Phys. Rev. Lett. **68**, 580 (1992).

[75] R. Dum, P. Zoller, and H. Ritsch, Monte Carlo simulation of the atomic master equation for spontaneous emission, Phys. Rev. A **45**, 4879 (1992).

[76] A. Barchielli and V. P. Belavkin, Measurements continuous in time and a posteriori states in quantum mechanics, J. Phys. A: Math. Gen. **24**, 1495 (1991).

[77] N. Gisin and I. C. Percival, The quantum-state diffusion model applied to open systems, J. Phys. A: Math. Gen. **25**, 5677 (1992).

[78] W. Casteels and M. Wouters, Optically bistable driven-dissipative Bose-Hubbard dimer: Gutzwiller approaches and entanglement, Phys. Rev. A **95**, 043833 (2017).

[79] H. Pichler, A. J. Daley, and P. Zoller, Nonequilibrium dynamics of bosonic atoms in optical lattices: Decoherence of many-body states due to spontaneous emission, Phys. Rev. A **82**, 063605 (2010).

[80] H. Pichler, J. Schachenmayer, A. J. Daley, and P. Zoller, Heating dynamics of bosonic atoms in a noisy optical lattice, Phys. Rev. A **87**, 033606 (2013).

[81] S. Diehl, A. Tomadin, A. Micheli, R. Fazio, and P. Zoller, Dynamical Phase Transitions and Instabilities in Open Atomic Many-Body Systems, Phys. Rev. Lett. **105**, 015702 (2010).

[82] A. J. Daley, J. M. Taylor, S. Diehl, M. Baranov, and P. Zoller, Atomic Three-Body Loss as a Dynamical Three-Body Interaction, Phys. Rev. Lett. **102**, 040402 (2009).

[83] P. Barmettler and C. Kollath, Controllable manipulation and detection of local densities and bipartite entanglement in a quantum gas by a dissipative defect, Phys. Rev. A **84**, 041606 (2011).

[84] S. L. Braunstein and C. M. Caves, Statistical Distance and the Geometry of Quantum States, Phys. Rev. Lett. **72**, 3439 (1994).

[85] L. Pezzè, A. Smerzi, M. K. Oberthaler, R. Schmied, and P. Treutlein, Quantum metrology with nonclassical states of atomic ensembles, Rev. Mod. Phys. **90**, 035005 (2018).

[86] L. Pezzé and A. Smerzi, Entanglement, Nonlinear Dynamics, and the Heisenberg Limit, Phys. Rev. Lett. **102**, 100401 (2009).

[87] G. Tóth, Multipartite entanglement and high-precision metrology, Phys. Rev. A **85**, 022322 (2012).

[88] P. Hyllus, W. Laskowski, R. Krischek, C. Schwemmer, W. Wieczorek, H. Weinfurter, L. Pezzé, and A. Smerzi, Fisher information and multiparticle entanglement, Phys. Rev. A **85**, 022321 (2012).

[89] G. Tóth and F. Fröwis, Uncertainty relations with the variance and the quantum Fisher information based on convex decompositions of density matrices, Phys. Rev. Res. **4**, 013075 (2022).

[90] M. G. A. PARIS, Quantum estimation for quantum technology, Int. J. Quantum Inf. **07**, 125 (2009).

[91] D. Šafránek, Discontinuities of the quantum Fisher information and the Bures metric, Phys. Rev. A **95**, 052320 (2017).

[92] D. Malpetti and T. Roscilde, Quantum Correlations, Separability, and Quantum Coherence Length in Equilibrium Many-Body Systems, Phys. Rev. Lett. **117**, 130401 (2016).

[93] P. Hauke, M. Heyl, L. Tagliacozzo, and P. Zoller, Measuring multipartite entanglement through dynamic susceptibilities, Nat. Phys. **12**, 778 (2016).

[94] I. Frérot, A. Rançon, and T. Roscilde, Thermal Critical Dynamics from Equilibrium Quantum Fluctuations, Phys. Rev. Lett. **128**, 130601 (2022).

[95] T. Kuwahara and K. Saito, Exponential Clustering of Bipartite Quantum Entanglement at Arbitrary Temperatures, Phys. Rev. X **12**, 021022 (2022).

[96] M. Van Regemortel, O. Shtanko, L. P. García-Pintos, A. Deshpande, H. Dehghani, A. V. Gorshkov, and M. Hafezi, Monitoring-induced entanglement entropy and sampling complexity, Phys. Rev. Res. **4**, L032021 (2022).

[97] J. Fricke, Transport equations including many-particle correlations for an arbitrary quantum system: A general formalism, Ann. Phys. (N. Y) **252**, 479 (1996).

[98] V. E. Colussi, H. Kurkjian, M. Van Regemortel, S. Musolino, J. van de Kraats, M. Wouters, and S. J. J. M. F. Kokkelmans, Cumulant theory of the unitary Bose gas: Prethermal and Efimovian dynamics, Phys. Rev. A **102**, 063314 (2020).

[99] V. E. Colussi, J. P. Corson, and J. P. D'Incao, Dynamics of Three-Body Correlations in Quenched Unitary Bose Gases, Phys. Rev. Lett. **120**, 100401 (2018).

[100] F. Caruso, C. Verdi, and F. Giustino, in *Handbook of Materials Modeling: Methods: Theory and Modeling*, edited by W. Andreoni and S. Yip (Springer International Publishing, Cham, 2020), p. 341.

[101] M. Sánchez-Barquilla, R. E. F. Silva, and J. Feist, Cumulant expansion for the treatment of light–matter interactions in arbitrary material structures, J. Chem. Phys. **152**, 034108 (2020).

[102] i. m. c. Özönder, Cumulant expansion in gluon saturation and five- and six-gluon azimuthal correlations, Phys. Rev. D **96**, 074005 (2017).

[103] A. Erschfeld, S. Floerchinger, and M. Rupprecht, General relativistic nonideal fluid equations for dark matter from a truncated cumulant expansion, Phys. Rev. D **102**, 063520 (2020).

[104] V. Mohanty, E. T. McKinnon, J. A. Helpern, and J. H. Jensen, Comparison of cumulant expansion and q-space imaging estimates for diffusional kurtosis in brain, Magn. Reson. Imaging **48**, 80 (2018).

[105] R. Schack and A. Schenzle, Moment hierarchies and cumulants in quantum optics, Phys. Rev. A **41**, 3847 (1990).

[106] H. A. M. Leymann, A. Foerster, and J. Wiersig, Expectation value based equation-of-motion approach for open quantum systems: A general formalism, Phys. Rev. B **89**, 085308 (2014).

[107] W. Casteels, S. Finazzi, A. L. Boité, F. Storme, and C. Ciuti, Truncated correlation hierarchy schemes for driven-dissipative multimode quantum systems, New J. Phys. **18**, 093007 (2016).

[108] T. C. H. Liew and V. Savona, Multipartite polariton entanglement in semiconductor microcavities, Phys. Rev. A **84**, 032301 (2011).

[109] F. Tonielli, R. Fazio, S. Diehl, and J. Marino, Orthogonality Catastrophe in Dissipative Quantum Many-Body Systems, Phys. Rev. Lett. **122**, 040604 (2019).

[110] P. Kirton and J. Keeling, Suppressing and Restoring the Dicke Superradiance Transition by Dephasing and Decay, Phys. Rev. Lett. **118**, 123602 (2017).

[111] D. Plankensteiner, C. Hotter, and H. Ritsch, QuantumCumulants.jl: A Julia framework for generalized mean-field equations in open quantum systems, Quantum **6**, 617 (2022).

[112] F. Robicheaux and D. A. Suresh, Beyond lowest order mean-field theory for light interacting with atom arrays, Phys. Rev. A **104**, 023702 (2021).

[113] J. Marino, Y. E. Shchadilova, M. Schleier-Smith, and E. A. Demler, Spectrum, Landau–Zener theory and driven-dissipative dynamics of a staircase of photons, New J. Phys. **21**, 013009 (2019).

[114] R. Christie, J. Eastman, and E.-M. Graefe, Quantum-jump vs stochastic Schrödinger dynamics for Gaussian states with quadratic Hamiltonians and linear Lindbladians, (2022), ArXiv:2203.11530.

[115] J. Marcinkiewicz, Sur une propriété de la loi de Gauß, Math. Z. **44**, 612 (1939).
[116] J. F. Kenney and E. S. j. a. Keeping, *Mathematics of Statistics, by J.F. Kenney and E.S. Keeping. Part 2* (1961).
[117] A. K. Rajagopal and E. C. G. Sudarshan, Some generalizations of the Marcinkiewicz theorem and its implications to certain approximation schemes in many-particle physics, Phys. Rev. A **10**, 1852 (1974).
[118] A. Auerbach, *Interacting Electrons and Quantum Magnetism* (Springer, New York, 1994).
[119] N. Linden, S. Popescu, and W. K. Wootters, Almost Every Pure State of Three Qubits Is Completely Determined by Its Two-Particle Reduced Density Matrices, Phys. Rev. Lett. **89**, 207901 (2002).
[120] N. Linden and W. K. Wootters, The Parts Determine the Whole in a Generic Pure Quantum State, Phys. Rev. Lett. **89**, 277906 (2002).
[121] D. L. Zhou, Irreducible Multiparty Correlations in Quantum States without Maximal Rank, Phys. Rev. Lett. **101**, 180505 (2008).
[122] M. Kardar, *Statistical Physics of Fields* (Cambridge University Press, Cambridge, 2007).
[123] I. Frérot and T. Roscilde, Quantum Critical Metrology, Phys. Rev. Lett. **121**, 020402 (2018).
[124] D. J. Wineland, J. J. Bollinger, W. M. Itano, and D. J. Heinzen, Squeezed atomic states and projection noise in spectroscopy, Phys. Rev. A **50**, 67 (1994).
[125] A. Sørensen, L.-M. Duan, J. I. Cirac, and P. Zoller, Many-particle entanglement with Bose–Einstein condensates, Nature **409**, 63 (2001).
[126] B. Zeng, X. Chen, D.-L. Zhou, and X.-G. Wen, *Quantum Information Meets Quantum Matter: From Quantum Entanglement to Topological Phases of Many-Body Systems* (Springer, Berlin, 2019).
[127] J. Tindall, A. Searle, A. Alhajri, and D. Jaksch, Quantum physics in connected worlds, (2022).
[128] M. Wouters, Quantum trajectories for the variational description of closed systems: A case study with Gaussian states, Phys. Rev. E **102**, 043314 (2020).
[129] A. D. Somoza, O. Marty, J. Lim, S. F. Huelga, and M. B. Plenio, Dissipation-Assisted Matrix Product Factorization, Phys. Rev. Lett. **123**, 100502 (2019).
[130] L. Fernandes, M. Wouters, and J. Tempere, Gaussian trajectory description of fragmentation in an isolated spinor condensate, Phys. Rev. A **105**, 013305 (2022).
[131] M. V. T. Grigori and N. Milstein, *Stochastic Numerics for Mathematical Physics*, 2nd ed., Scientific Computation (Springer Nature Switzerland AG, 2021).